Short title: Microdomain coordination between neighbors in plants

Authors:

Andreas Kolbeck[1,4], Peter Marhavý[1,4,5¶], Damien De Bellis[1,2], Baohai Li[3,6], Takehiro Kamiya[3], Toru Fujiwara[3], Lothar Kalmbach[1,†] and Niko Geldner[1,§,‡]

Title: CASP microdomain formation requires cross cell wall stabilization of domains and non-cell autonomous action of LOTR1

Author affiliations and footnotes

1 Department of Plant Molecular Biology, University of Lausanne, Lausanne, Switzerland

2 Electron Microscopy Facility, University of Lausanne, Lausanne, Switzerland

3 Department of Applied Biological Chemistry, The University of Tokyo, Tokyo, Japan

4 These authors contributed equally

5 Present address: Umeå Plant Science Centre (UPSC), Department of Forest Genetics and Plant Physiology, Swedish University of Agricultural Sciences (SLU), Umeå, Sweden

6 College of Environmental and Resource Sciences, Zhejiang University, China

7 Present address: Sainsbury Laboratory, University of Cambridge, Bateman Street, Cambridge CB2 1LR, UK

8 Corresponding author. Tel: +41 21 692 4192;

E-mail: niko.geldner@unil.ch

Summary

Efficient uptake of nutrients in both animal and plant cells requires tissue-spanning diffusion barriers separating inner tissues from the outer lumen/soil. However, we poorly understand how such contiguous three-dimensional superstructures are formed in plants. Here, we show that correct establishment of the plant Casparian Strip (CS) network relies on local neighbor communication. We show that positioning of Casparian Strip membrane domains (CSDs) is tightly coordinated between neighbors in wild-type and that restriction of domain formation involves the putative extracellular protease LOTR1. Impaired domain restriction in *lotr1* leads to fully functional CSDs at ectopic positions, forming "half strips" LOTR1 action in the endodermis requires its expression in the stele. LOTR1 endodermal expression cannot complement, while cortex expression causes a dominant-negative phenotype. Our findings establish *LOTR1* as a crucial player in CSD positioning acting in a directional, non-cell-autonomous manner to restrict and coordinate CS positioning.

Keywords

Endodermis, Casparian Strips, extracellular diffusion barriers, membrane domains, coordination, cell ablation

48 **Introduction**

49 Plants mine the surrounding soil for water and dissolved minerals to
50 sustain their growth and to complete their life cycle. Likened to inverted
51 guts, roots evolved crucial epithelial functions — selective uptake and
52 diffusion barriers — in order to generate and sustain body homeostasis in
53 variable and harsh environments. In gut epithelial cells, the required
54 separation of outside lumen and inside tissues is achieved through the
55 formation of tight junctions. These specialized membrane domains form
56 ring-like domains between the apical (gut lumen) and basal (blood stream)
57 sides. Close adhesion of both adjacent plasma membranes is achieved by
58 tight interaction of occludins, claudins, and cadherins, organized into tight
59 and adherens junctions, forming impermeable and mechanically-resistant
60 barriers. In plants, a functionally similar diffusion block is achieved by
61 Casparian strips (CS), highly localized impregnations of the cell wall, the
62 plant's extracellular matrix, in root endodermal cells.

63 Similar to tight/adherence junctions, a specialized membrane domain
64 (Casparian Strip membrane Domain, CSD) forms a precise ring in
65 transversal and anticlinal membranes of elongated endodermal cells. This
66 domain acts as a molecular fence that separating the endodermal plasma
67 membranes into peripheral (outer) and central (inner) domains,
68 highlighted by the polar distribution of nutrient transporters (Julien
69 Alassimone, Naseer, and Geldner 2010; Bao et al. 2019; Ma et al. 2007;
70 Takano et al. 2010). CASPARIAN STRIP DOMAIN PROTEINs (CASPs) are
71 specifically targeted to this domain and form a stable matrix for the
72 subsequent lignification machinery (Roppolo et al. 2011; Lee et al. 2013;
73 Hosmani et al. 2013; Kalmbach et al. 2017; Barbosa, Rojas-Murcia, and
74 Geldner 2019). Lignification of the primary cell wall of CSs extends through
75 the entire apoplast including cross-linkage to the middle lamella. This is
76 illustrated in cell wall digestions leaving only the resistant lignified tissues
77 of CSs and xylem visible as a fishnet-like matrix (Enstone, Peterson, and Ma
78 2002).

79 The CS and tight/adherens junctions must form a contiguous network in
80 order to fulfill their role as functional diffusion barriers. However, we still
81 poorly understand how such a supracellular structure is coordinated within
82 the endodermal cell layer. Although we are ignorant of the mechanism, the
83 precisely opposing localization of CSDs evidences that endodermal cells
84 coordinate the positioning of their membrane domains across the cell wall
85 space. In epithelial cells, adherens junctions are first initiated by cell-to-cell
86 contact mediated by nectins and cadherins and kept in place by firm
87 attachment to the actin cytoskeleton (Rajasekaran et al. 1996; Itoh and
88 Bissell 2003). In plant cells, their cell wall matrices separate neighboring
89 cell by at least 100-200 nm, which prevents such a direct interaction of
90 membrane bound proteins. Thus, a more complex positioning mechanism
91 that requires local signals from directly adjacent neighbors could ensure
92 coordination of CSDs between neighbors.

93 Many components necessary for correct CS formation have been identified
94 in recent years, but few show impacts on CS positioning *per se*. Mutation of
95 components in the recently discovered barrier surveillance mechanism
96 causes interrupted, but correctly localized CSDs (Pfister et al. 2014; Doblas
97 et al. 2017; Nakayama et al. 2017; J Alassimone et al. 2016). Loss of the
98 endodermal differentiation transcription factor MYB36 abolishes the
99 formation of the entire CSD while disruption of CS cell wall localised ESB1
100 causes unstable, but still correctly localised domains (Kamiya et al. 2015;
101 Liberman et al. 2015; Hosmani et al. 2013). The recently published *lotr2*
102 mutant revealed the importance of a member of the exocyst complex,
103 *EXO70A1*, in mediating targeted secretion of CASP proteins to the pre-
104 established CSD (Kalmbach et al. 2017). However, the fragmented domains
105 visible in this mutant are non-functional and unstable. Thus, based on
106 current data, it is unclear whether formation of functional CSDs at ectopic
107 positions is even possible.

108 Here, we report that the recently discovered *lotr1* mutant forms fully
109 functional CSDs outside the endodermal-endodermal cell interface in. We
110 establish that neighbouring endodermal cells are absolutely required to

111 form stable and continuous CSDs and we highlight close coordination of
112 CSD microdomains during the early stages of domain formation. In
113 addition, we demonstrate that *LOTR1* is crucial for restriction of the CSD
114 and that it acts independently of any known pathway for CSD formation.
115 We show that this new type of putative cell wall protease is expressed in
116 the stele, represents a novel, non-cell-autonomous and directional
117 signalling component that controls CSD stability in the endodermis. Thus,
118 we demonstrate that signalling, both within and between cell layers is
119 crucial for coordinating CS positioning.

120

121 **Results**

122 *Ectopic CASP deposits in lotr1 are fully functional CSDs*

123 During their initial characterization of the *lotr1* mutant, Li et al. 2017
124 reported a novel 'patchy' phenotype, where large patches of the Casparian
125 strip membrane domain marker CASP1::CASP1-GFP occurred outside of the
126 regular median CS position. Further analysis revealed an apoplastic delay
127 phenotype attributed to large gaps that could be observed in the CS upon
128 lignin stain. We performed a more detailed analysis of the domain marker
129 CASP1::CASP1-GFP in this mutant background to search for disruptions in
130 the CSD that could explain these gaps in lignification. Confirming the earlier
131 findings (Li et al. 2017), we found large patches of CASP1-GFP occurring in
132 endodermal membranes that were never observed in wildtype plants (Fig.
133 1B). Whereas previously reported to occur only facing pericycle cells, we
134 found similar patches to also occur towards the outer cortex (Fig. 1B, Fig.
135 S1A), although quantification revealed a clear preference for the
136 endodermal-pericycle interface (Fig. S1B). In addition to these patches, we
137 found disruptions of the central CSD which occurred primarily at cell
138 corners with nearby ectopic CASP deposits (Fig. 1B), coherent with the
139 reported gaps in CS lignin. The overall correctly positioned and largely
140 continuous central CSD in *lotr1* suggests that the core-localization
141 mechanism for the CSD is still functional. We speculate that the change in
142 cell shape and cell walls at junctions might favor patch formation in *lotr1*. If

143 patch formation starts simultaneously with initial focalization of CASPs into
144 micro-domains (known as the string-of-pearls stage), nearby ectopic CASP
145 deposits might inhibit the growth of the central domain leading to the
146 observed large discontinuities. In order to better understand the nature
147 and origin of these patches, we followed CASP deposition throughout
148 endodermal differentiation. In both wildtype and *lotr1*, CASP1-GFP
149 aggregated into aligned micro-domains in the cell's median (Fig. S1C).
150 During this initial focalization step, we observed occurrence of ectopic
151 CASP islands in *lotr1*, indicating a role of LOTR1 during this early step of
152 defining the CS location. Ectopic CASP deposits grew over time and were
153 able to fuse into larger patches, similarly to the central micro-domains
154 combining into a continuous ring. We did not observe degradation of these
155 patches nor formation of new patches once the central domain was fused,
156 confirming that these patches are stable once formed and their
157 establishment is restricted to the short developmental window in which
158 the cells determine their CS location. Consequently, LOTR1 likely acts in
159 this early phase as an inhibitor of ectopic domain formation. We then
160 investigated whether these patches represent fully functional domains, i.e.
161 whether they are able to guide lignification enzymes to these sites.
162 Deposition of lignin can be easily identified in electron microscopy, where
163 CSs are visible as a clearly defined, homogenous stretch of cell wall
164 spanning the entire apoplastic space (Roppolo et al. 2011; Fujita et al.
165 2020) (Fig. S1D). Ultra-structure analysis of *lotr1* revealed similar cell wall
166 modifications in pericycle-facing endodermal membranes (Fig. 1D).To our
167 surprise, and in contrast to regular CSs, this ectopic lignin patch was
168 restricted to the endodermal part of the cell wall, stopping precisely at the
169 middle lamella, effectively creating half of a Casparian Strip. Such a strict
170 spatial confinement of lignification on a nanometer scale is quite surprising
171 since monolignols and ROS, both essential for lignin polymerization, are
172 thought to be mobile in cell walls and lignin polymerization itself not to be
173 under direct enzymatic control. To our knowledge, such a strictly restricted
174 lignification encompassing only half of a thin primary has not been
175 observed previously. Our finding therefore suggests a very local and

176 directed lignin polymerization in the CS, where each endodermal cell is
177 responsible for lignifying their part of the cell wall to build a functional CS
178 barrier. A functional CSD is also characterized by a tight attachment of the
179 underlying membrane, which is revealed in EM by the mild plasmolysis of
180 the plasma membrane introduced through sample preparation, and which
181 is absent at the CSD. Perfectly matching the cell autonomous nature of the
182 ectopic patches, tight attachment of the endodermal plasma membrane,
183 but not the pericycle plasma membrane was observed.

184 In order to further support our hypothesis that *lotr1* ectopic patches are
185 fully functional domains, we compared consecutive electron micrograph
186 sections with and without potassium permanganate ($KMnO_4$) staining to
187 check for lignification. Depositing electron dense material by reaction with
188 lignin sidechains, $KMnO_4$ highlights lignin presence as darkening of cell
189 walls in Casparian strips and protoxylem vessels (Stein, Klomparens, and
190 Hammerschmidt 1992; Yamashita et al. 2016). Ectopic patches in *lotr1*
191 displayed KMnO4 staining on the endodermal side of the half-strips, while
192 the opposite pericycle cell walls were unstained (Fig. 1E). This correlated
193 with CS-typical cell wall appearance (more homogenous, less electron-
194 dense, slightly thickened) observed in unstained consecutive cuts,
195 confirming lignin presence at these ectopic domains. Notably, several
196 samples displayed CS-type cell wall morphology with accompanying
197 membrane attachment and lignification throughout the entire endodermal
198 cell corner, stretching from the median endodermal-cell interface all the
199 way to the endodermal-pericycle cell walls (Fig. S1E). Although ectopic
200 lignification is a hallmark of many Casparian Strip mutants, this was not
201 described for *lotr1*. Furthermore, enhanced lignification itself does not
202 result in firm membrane attachment outside the regular CS. Consequently,
203 this points to a drastically enlarged CSD indicative of an impaired ability to
204 restrict CSD growth in *lotr1,* agreeing with a presumed role of LOTR1 as
205 inhibitor of domain formation.

206 The regular CSD recruits a multitude of enzymes required for restricted
207 monolignol polymerization to form the CS. The tightly restricted lignin

208 accumulation at ectopic *lotr1* patches suggested similar recruitment of
209 these enzymes. Indeed, when we co-expressed the CSD marker CASP1-GFP
210 together with typical members of this lignin machinery in *lotr1* to confirm
211 their recruitment to ectopic CSDs. Endodermis specific PEROXIDASE 64
212 (PRX64) and LACCASE 3 (LAC3) displayed a clear co-labelling in both central
213 and ectopic domains while NADPH oxidase RbohF, the main generator of
214 ROS for monolignol polymerization, was also found to be present, although
215 it did not specifically accumulate there (Fig. 1F). Finally, we analyzed the
216 localization of dirigent-domain protein ESB1 in *lotr1*. Although it was
217 previously reported to be absent from ectopic deposits (Li et al. 2017). We
218 found ESB1 to accumulate at the sites of ectopic CASP1-deposition when
219 expressed as ESB1-mCherry under its native promoter together with
220 CASP1-GFP. Dirigent-domain proteins are thought to be a key component
221 in restricting and directing lignin polymerization in the cell wall (Hosmani et
222 al. 2013). Our results of ESB1 localization therefore agree with PER64 and
223 LAC3 labelling, as well as the tight restriction of lignin at these patches,
224 proving these ectopic formations to be fully functional, but ectopically
225 formed CSDs.

226 *Focalization of CASPs is coordinated between cells*

227 The fact that an ectopic CSD patch towards a non-endodermal neighbor
228 can only induce formation of a half-strip suggested that two neighboring
229 endodermal cells absolutely need to align their respective CSDs in order to
230 lignify the entire CS cell wall space. To ensure this, a mechanism would
231 need to be in place that promotes formation of a CSD at places where a
232 neighboring cell is forming one and/or inhibits CSD formation in the
233 absence of a neighboring CSD. We therefore investigated the initial
234 focalization of CASP proteins at high resolution. When properly aligned
235 along the z-axis, we were able to identify two distinct membrane signals
236 present between two neighboring endodermal cells (Fig. 2A,C). Strikingly,
237 at the string-of-pearls stage, CASP1-GFP intensity along the length of both
238 signals already showed a strong positive correlation (R^2 = 0.535, p = 1.612
239 e-9) (Fig. 2B), indicating coordination of CSD formation across the cell wall

240 already at this stage. To validate our assumption that these paired signals
241 represent the signals of neighboring cell membrane domains, we checked
242 the position of CS cell wall protein ESB1 and cell wall tracer Propidium
243 Iodide (Fig. 2C,D). In contrast to CASP1-GFP, ESB1-mCherry localized in a
244 single line in between the observed CASP-labelled membranes in both early
245 and late CSDs (Fig. 2C). To further confirm that these GFP signals truly
246 represented separate membranes, we decided to employ cell-specific laser
247 ablation to destroy one of the cells, arguing that this should remove only
248 one half of the paired signal. Indeed, upon ablation, GFP signal was
249 specifically lost in the ablated cell whereas the adjacent signal of the intact
250 neighboring cell was unchanged (Fig. 2D,E). Together, our data
251 demonstrate the observed double signals to be adjacent CSDs of
252 neighboring endodermal cells, whose initial formation is tightly
253 coordinated between cells. We then investigated whether currently known
254 mutants such as *sgn1*, *sgn3* and *esb1* would display defects in CASP
255 microdomain coordination (Fig. S2A). However, all these mutants showed
256 wildtype like coordination between adjacent CSDs. Interestingly, *lotr1* also
257 showed well-coordinated deposition of micro-domains at the Casparian
258 strip position. Therefore, while LOTR1 appears to be necessary to restrict,
259 unpaired, ectopic domain establishment, its loss-of function does not seem
260 to affect the process of coordination at the correct central position where
261 the future CS between neighboring cells is forming. This is corroborated by
262 the lack of CS half-strips at the regular median position between
263 endodermal cells in *lotr1 (Fig. S2A)*.

264 *Endodermal cells require a neighboring cell to stabilize CASPs*

265 The close correlation of CASP micro-domains in neighboring endodermal
266 membranes could be explained by an unknown feedback control
267 mechanism that stabilizes microdomains upon presence of neighboring
268 domains and de-stabilizes them in their absence. Such a mechanism would
269 immediately guide CSD formation towards endodermis-endodermis
270 surfaces. In order to test this model, we ablated individual endodermal
271 cells in the elongation zone, prior to their transition to differentiation. This

272 enabled us to compare CSD establishment with and without a functional
273 neighbor in the same cell. Initially, we observed CASP deposition in a string-
274 of-pearls-typical pattern in membranes facing living and dead cells alike
275 (Fig. 3A,D). However, only membranes facing intact neighbors were able to
276 form a continuous strip, whereas domains towards ablated cells did not
277 progress past the string-of-pearls stage. When we ablated all adjacent cells,
278 the single intact cell was still able to express and focalize CASPs but was
279 unable to establish any continuous domains (Fig. 3C). We also noticed a
280 strong difference in signal intensity between membranes facing living and
281 dead cells, where GFP signal increased rapidly in CSDs towards intact
282 neighbors, but not ablated cells (Fig. 3B). This discrepancy is likely a result
283 of an inability to recruit additional CASP proteins to the initially formed
284 micro-domains. This suggested a control point during CSD establishment
285 where a neighboring signal is required to progress from the string-of-pearls
286 stage and commit to formation of a CS. We had to exclude that isolating
287 endodermal cells from their neighbors by ablation might cause stresses
288 that influence overall endodermal differentiation and not just a
289 destabilization of CASP recruitment to the membrane. We therefore used a
290 CASP1 transcriptional reporter, driving a nuclear fluorescent protein. Upon
291 ablation of all surrounding endodermal cells a similar CASP promoter
292 activity compared to non-affected cells was observed, indicating that
293 progress of differentiation *per se* was not halted in the isolated cell (Fig.
294 S3A). To rule out possible general effects on secretion or localization of
295 plasma membrane proteins, we then ablated cells in double marker lines
296 expressing CASP1-GFP and the generic SYP122-3xmCherry plasma
297 membrane marker, both under the control of the CASP1 promoter. Again,
298 this clearly established that isolated cells still express from the CASP1
299 promoter. Moreover, they accumulate SYP122 on all cell sides, in contrast
300 to CASP1, which accumulates only at plasma membrane domains facing a
301 living neighbor (Fig. 3D).

302 We then thought to confirm our findings by means that do not involve
303 destruction of neighboring cells. To do so we generated inducible

304 complementation lines for MYB36, a key transcription factor of
305 endodermal differentiation (Liberman et al. 2015; Kamiya et al. 2015).
306 *myb36* loss-of-function mutants are unable to activate expression of key
307 CSD proteins, e.g. CASPs, and consequently lack a CSD. Using very low level
308 of inducer, we generated sporadic MYB36 activation to enable some, but
309 not all cells to start differentiation and initiate CS formation. Expectedly,
310 we observed a sporadic, patchy expression pattern of CSD domain marker
311 CASP1-GFP upon induction, with some samples displaying expression in
312 isolated, single cells, while others showed cell groups with a near complete
313 CSD network (Fig. 3E). Confirming our ablation results, we found that
314 isolated cells were able to deposit CASP1-GFP in typical micro-domains but
315 were incapable of forming a stable and continuous CSD, similar to what
316 was observed using cell ablation (Fig. 3E, left). If two adjacent cells started
317 to deposit CASPs, we observed an increase in GFP signal only in the domain
318 between these cells, followed by fusion of the initial micro-domains into a
319 continuous strip (Fig. 3E, right). The domains not facing a CASP1 expressing
320 neighbor did not progress beyond a string-of-pearls stage and eventually
321 lost the CASP1-GFP signal (Fig. 3F, S3B). We conclude that wildtype plants
322 appear to require signals from neighbors to form stable microdomains and
323 commit to a CS. *lotr1* is currently the only known mutant that can form
324 functional microdomains in the absence of neighbors. We therefore asked
325 whether *lotr1* might be able to fuse micro-domains at the side facing the
326 dead neighbor into continuous strips. Yet, when we ablated cells in *lotr1,*
327 we observed a similar disappearance of the central CSD facing the ablated
328 cell (Fig S3C). One explanation could be that LOTR1 function is redundant
329 for destabilization of unpaired domains in the correct, central position, but
330 is required at surfaces facing non-endodermal neighbors. Indeed, we did
331 observe formation of stable, *lotr1*-typical patches on the side facing its
332 dead neighbor, although they occurred in membranes facing living
333 pericycle cells.

334 *LOTR1 defines a novel pathway controlling CASP domain positioning*

335 While no other knock-out mutant resembles *lotr1*, overstimulation of the
336 SCHENGEN (SGN) pathway by external application of CIF2 peptide, leads to
337 ectopic formation of CASP domains somehow resembling the phenotype of
338 *lotr1*. The CIF2 peptide is perceived by the Leucine-rich repeat receptor
339 kinase SGN3 (also called GSO1), a key receptor controlling a novel
340 apoplastic barrier surveillance pathway (Doblas et al. 2017; Nakayama et
341 al. 2017). A complete absence of SGN3 activity in knock-out mutants leads
342 to an incomplete fusion of otherwise correctly positioned CASP micro-
343 domains. In order to test, whether *lotr1* ectopic patches are due to an
344 overactive SGN pathway, we generated double knockouts of *lotr1* in
345 combination with *sgn1*, *sgn2* or *sgn3*. Single mutants *sgn1* and *sgn2*
346 showed sporadic disruptions in their central CSD while *sgn3* displayed
347 more numerous holes in comparison, agreeing with previously published
348 data (J Alassimone et al. 2016; Doblas et al. 2017) (Fig. 4A). Double mutants
349 displayed *lotr1*-typical ectopic deposition of CASP1-GFP, as well as
350 discontinuities of the central domain. Although discontinuities in the
351 central CSDs were visible in *lotr1* itself, these occurred mostly at cell
352 junctions, while *sgn*-typical interruptions were present throughout the
353 length of the CSD. Both types of disruptions were found in the respective
354 double mutants. Moreover, no significant difference between the double
355 and single mutants was observed in blockage of apoplastic tracer PI, a test
356 for CS functionality (Fig 4C). This clear additivity of phenotypes suggests
357 that LOTR1 and SGN mutants are involved in separate pathways. It
358 certainly excludes a model whereby ectopic patch formation of *lotr1* is due
359 to an overactive SGN pathway. We also tested a possible connection to
360 ESB1. Again, *lotr1 esb1* double mutants displayed a addition of parental
361 phenotypes with an *esb1*-typical string-of-pearl-stage central CSD and
362 *lotr1*-typical ectopic CASP deposits and showed no enhanced apoplastic
363 barrier phenotype, indicating that LOTR1 also acts independently of esb1 in
364 CS domain formation.

365 The model of SGN3-CIF1/2 integrity signaling predicts enhanced
366 lignification of endodermal cell corners and an early onset of suberization

367 whenever the diffusion barrier is broken in such a way that CIF peptides
368 cannot be restricted anymore. The previously described enhanced suberin
369 phenotype in *lotr1* is consistent with such a barrier-defect induced
370 activation of the SGN pathway, due to its large corner gaps in the CS
371 domain. The previously reported large gaps in lignification of CSs (Li et al.,
372 2017), fit the discontinuous CSDs in this mutant. Presence of $KMnO_4$-
373 stained lignin throughout the endodermal cell corners found in some
374 samples during our ultra-structural analysis (Fig. S1E) resembled SGN3-
375 induced ectopic lignification. To unambiguously demonstrate ectopic lignin
376 deposition outside the CASP-labelled domain, we employed a novel
377 clearing protocol that enables co-observation of fluorescent markers, e.g.
378 CASP1-GFP, and lignin specific stains, such as Basic Fuchsin (Ursache et al.
379 2018) (Fig. S4A). As described, in addition to the central CS, lignin
380 accumulates at ectopic CASP1-deposits in *lotr1* (FIG 4B). However, cell
381 corner lignification not associated with CASP1 domains was observed at
382 sites of gaps in the CSD, but not at places where the CSD was continuous.
383 This nicely supports the recently proposed model in which SGN3-
384 stimulation can induce local lignification with subcellular precision (Fujita
385 et al. 2020). Consistently, enhanced lignin deposition in cell corners was
386 not present in the *lotr1 sgn3* double mutant, confirming that this ectopic
387 lignin is caused by activation of the barrier surveillance mechanism. *lotr1*-
388 typical patches, by contrast, were still lignified in the double mutant,
389 supporting the concept of two separate pathways controlling lignin
390 deposition in the endodermis: A developmental lignification pathway
391 building up CS-type lignin and the SGN3-mediated ectopic lignin deposition
392 that compensates in case of barrier defects. Exogenous application of CIF2
393 peptide further demonstrated that the SGN3-pathway is functional in *lotr1*
394 (Fig. 4D). In the presence of CIF2, both genotypes formed ectopic lignin at
395 cell corners.

396 *LOTR1 is broadly expressed in the root*

397 Due to a lack of available expression data in public databases (*LOTR1* was
398 not included on the ATH1 microarrays), it was crucial to generate a

399 reporter line. We therefore placed a nuclear-localized tdTomato under the
400 control of a 3 kb LOTR1 promoter fragment. We observed strong promoter
401 activity in the root meristem in nearly all tissue layers and cells, including
402 QC and columella, with the highest expression found in the stele (FIG 4E).
403 Very low expression was found in the epidermis and ground cell lineage,
404 with promoter activity visible in cortex/endodermal initials and their
405 endodermis daughter cells, but not in the cortex daughter. In older
406 meristematic cells, *LOTR1* expression further reduced in epidermis and
407 endodermis, whereas stele cells continued to show strong promoter
408 activity. This pattern continued past the elongation zone, where stele
409 expression was still strong with some residual signals found in epidermal
410 and endodermal cells. Inside the stele itself, *LOTR1* was specifically absent
411 in xylem precursor and xylem-adjacent procambium cells, whereas
412 pericycle, phloem precursor and phloem-adjacent procambium cells
413 displayed strong expression (FIG 4E). Recently published single-cell RNA
414 sequencing results showed strong expression of LOTR1 in clusters
415 corresponding to phloem, stele, xylem, and root cap cells, confirming our
416 promoter activity analysis (Ryu et al. 2019; Denyer et al. 2019). Despite this
417 broad expression pattern, *lotr1* mutants displayed only phenotypes related
418 to endodermal differentiation, i.e. ectopic CASP deposition and disrupted
419 CSDs causing compensatory lignification and suberin deposition, which
420 themselves are likely responsible for the previously observed delay in
421 lateral root development and low-calcium-sensitivity phenotype (Li et al.
422 2017). Consequently, if the expression pattern points to a much broader
423 function for LOTR1 outside of endodermal differentiation, these additional
424 functions are probably redundantly fulfilled some of the many homologs of
425 LOTR1 (Fig. 4F).

426 *LOTR1* codes for a putative cell wall protein with a predicted signal peptide,
427 a putative auto-inhibitory domain (Neprosin-AP), and a Neprosin domain,
428 recently identified as novel proline protease domain in an enzyme found in
429 the digestive fluids of pitcher plants (Rey et al. 2016; Schrader et al. 2017).
430 We found 42 other proteins in the Arabidopsis proteome with a domain

431 structure like LOTR1, i.e. having both Neprosin-AP and Neprosin domains,
432 although subsequent phylogenetic analysis showed considerable variation
433 among the family members. Average identity towards LOTR1 among this
434 "HOMOLOGS-OF-LOTR1" (HOLO) family was only 38 % (± 12) with the three
435 closest homologs standing out at ~ 70 % (Table S1). Phylogenetic clustering
436 identified 5 subgroups (A:E) with instances of gene-duplication events
437 visible especially in group C, where 8 homologs were found in consecutive
438 loci on chromosome 4, highlighting the variable nature of this family (Fig.
439 4F). Nevertheless, putative orthologs of LOTR1 can be identified in both
440 mono- and eudicot species, indicating that, although some family members
441 seem to evolve rapidly, LOTR1 has a deep conservation of function,
442 expected for a regulator of CS formation.

443 While 34 of the putative homologs showed predicted signal peptides for
444 apoplastic localization, we also found 5 proteins in the family predicted to
445 have a single N-terminal transmembrane domain with their active domain
446 outside in the apoplast (Fig. 4F, Table S1). Thus, the HOLO family are
447 interesting candidates for proteolytically processing membrane or cell wall
448 proteins relevant for domain establishment. Single-cell RNAseq expression
449 profiles of *LOTR1's* four closest homologs partially overlapped in cell
450 clusters for QC/meristem (At1g23340, At1g70550, At5g56530), root cap
451 (At1g10750, At1g70550), phloem (At1g70550, At5g56530), and xylem
452 (At1g10750, At23340, At1g70550, At56530) (Ryu et al. 2019), explaining
453 the lack of any meristematic phenotypes in *lotr1*. However, while 8
454 separate mutants with this unique patchy phenotype identified in the
455 *LORD-OF-THE-RINGS* screen all turned out to be alleles of *LOTR1*, none of
456 its homologs were found, indicating they likely have separate roles.

457 Mature and active Neprosin has been reported to consist only of its
458 functional domain (PF03080) (Rey et al. 2016), presumably undergoing
459 processing during or after secretion. However, only full-length protein was
460 found in functional, full-length complementation lines (Fig. S4C), suggesting
461 that LOTR1 might retain its putative auto-inhibitory Neprosin-AP domain.
462 Expression of artificially truncated versions of LOTR1 consisting of only its

463 Neprosin domain or only its putatively auto-inhibitory Neprosin-AP domain
464 resulted in extensive intracellular labelling and absence of
465 complementation (Fig. S4D), supporting that LOTR1 does not undergo post-
466 processing.

467 As many of the Neprosin-containing proteins are still annotated as putative
468 carboxyterminal proteases, we investigated potential homologies towards
469 such enzymes. Database searches identified *E.coli* protein mepS, a cell wall
470 protease required for cell wall expansion, as a potential candidate.
471 Although displaying only 20 % identity to LOTR1's Neprosin domain,
472 structural comparison revealed that three crucial amino acids in the
473 catalytic center of mepS, one cysteine and two histidines, are present in
474 LOTR1, its three closest homologs, as well as Neprosin itself (Fig. S5A,B).
475 Expression of a full-length LOTR1 version with putative active-site residues
476 C255 and C260 mutated to alanine showed apoplastic localization similar
477 to unmutated LOTR1, but was unable to complement the *lotr1* phenotype
478 (Fig. S4D). This suggests an important functional role for these amino acids
479 in LOTR1 and supports a protease function for this enzyme class in
480 *Arabidopsis*.

481 *Tissue specific complementation indicates a non-cell autonomous action for*
482 *LOTR1.*

483 The strong expression pattern of LOTR1 suggests a function in the inner
484 stele tissues and a non-autonomous action of LOTR1 on endodermal
485 differentiation. With a potential protease function an action on the equally
486 stele-expressed CIF peptides was conceivable, but inconsistent with our
487 genetic analysis. In order to establish the site of LOTR1 action, we
488 generated LOTR1 fusion proteins and were able to complement the loss-of-
489 function phenotype with LOTR1 N-terminal (behind the signal peptide), but
490 not C-terminal fusion proteins, indicating that a free C-terminus is
491 important for its functionality (Fig. 5A). Interestingly, the *lotr1-8* allele,
492 where a late STOP-codon truncated the protein by just 16 aa leads to a
493 knock-out phenotype, further suggesting an important role of the c-
494 terminal extremity. In agreement with the promoter activity, fluorescence

495 of the fusion construct was mainly visible in the apoplastic space between
496 stele cells, with outer tissues showing very low levels of accumulation (Fig.
497 5A).

498 To determine if the very low expression observed in the endodermis is
499 nonetheless responsible for LOTR1 function, we generated lines driving
500 LOTR1 expression from stele-, endodermal-, or cortex-specific promoters in
501 the *lotr1* mutant background. We found continuous CSDs and lack of
502 patches only when expressed from the stele specific SHORTROOT (SHR)
503 and CIF2 promoters, but not from endodermal SCR, CASP1, and ELTP, nor
504 cortex specific C1 promoters (Fig. 5C). Covering early, intermediate, and
505 late endodermal development, the lack of complementation by
506 endodermal promoters demonstrated that LOTR1 was not acting in the
507 endodermis to fulfil its role in CSD formation. Peculiarly, expression of the
508 same construct under the ubiquitous 35S CaMV promoter did also not
509 seem to complement the underlying *lotr1* phenotype. Several scenarios
510 could explain this finding: LOTR1 function could require exclusive
511 expression in the stele, although its native promoter showed some weak
512 outer tissue activity. Alternatively, over- and misexpression of the
513 construct might lead to the same patchy *lotr1* phenotype, but through
514 dominant interference. We therefore created an inducible
515 complementation construct, where the 3kb *LOTR1* promoter fragment was
516 fused to the estrogen-inducible artificial XVE transcription factor, with a
517 subsequent minimal 35S promoter driving expression of the native gene
518 (Zuo, Niu, and Chua 2000; Siligato et al. 2016). This allows control of
519 expression strength of the target genes. Upon induction of this construct in
520 the *lotr1* background, we observed a full complementation of the
521 phenotype even under strong induction conditions (Fig. 5B). Control plants
522 without inducer showed the typical phenotype. Thus, expression strength
523 was not causing the seeming absence of complementation in the 35S lines,
524 leaving mis- expression in outer tissues as a probable cause for the
525 observed phenotype.

526 We therefore tested whether ubiquitous expression via 35S would lead to
527 a dominant-interference phenotype in wildtype. We outcrossed all
528 generated lines to wildtype CASP1-GFP plants to test for genetic
529 dominance of the transformed constructs. Previously complementing
530 constructs LOTR1::LOTR1, SHR::LOTR1, and CIF2::LOTR1 continued to
531 display a wild-type CSDs and no occurrence of *lotr1* typical patches in the
532 F1 generation (Fig. 5C). Expectedly, wild-type phenotypes were also
533 observed for the non-complementing, endodermis-specific SCR and CASP1
534 driven lines. Remarkably, not only expression driven by 35S, but also from
535 cortex-specific C1 and endodermal/cortex-expressing ELTP promoters
536 caused ectopic CASP1-GFP patches like those observed in
537 uncomplemented *lotr1* in the F1 progeny. We confirmed this dominant
538 phenotype in the following segregating F2 generations, where all plants
539 harboring ELTP, C1, or 35S constructs showed patch formation. Only 7/37
540 (ELTP), 9/42 (C1), and 8/45 (35S) plants displayed wildtype like continuous
541 CSDs and no patches in the respective F2 populations. Since the dominant
542 phenotype was not easily distinguishable from the normal *lotr1* loss-of-
543 function phenotype, our observed ratios (18.9 %, 21.4 %, 17.7 %) matched
544 the expected 3/16 (18.75 %) Mendelian segregation ratio for a wildtype
545 phenotype (non *lotr1*-homozygous, plus absence of dominant transgene).
546 Apoplastic barrier functionality tests in these lines confirmed our
547 observations (Fig. 5D).

548

549 **Discussion**

550 Establishment of a functional apoplastic barrier relies on the correctly
551 localized deposition of lignin at the median position between endodermal
552 cells (Naseer et al. 2012; Geldner 2013). Although many components
553 involved in this process have been identified in the last decade, we still
554 poorly understand the mechanism by which these cells achieve the precise
555 formation of Casparian Strips in such a way that a single, thin, continuous
556 ring of lignin is formed in between endodermal cells. In our current work,
557 we provide new insights into this mechanism by demonstrating strict

558 coordination of CASP deposition in membranes of adjacent endodermal
559 cells. Independent of any known CS mutant, this coordination pathway
560 appears to allow a local initial pairing of forming CASP micro-domains,
561 across the cell wall of neighboring endodermal cells, which promotes their
562 stabilization and eventual fusion. This results in the necessity for having a
563 functional, differentiating endodermal cell neighbors in order to form a
564 continuous CS. Without a neighboring cell in the same developmental
565 state, wild-type endodermal cells abort CS development after the initial
566 formation of CASP microdomains, which eventually disappear. In our
567 current understanding, CASPs are initially secreted in a non-localized
568 fashion (Roppolo et al. 2011), yet rapidly form aligned CASP micro domains.
569 This is initiated by a specific exocyst complex, defined by subunit EXO70A1,
570 whose accumulation at the site of the future CS precedes CASP
571 accumulation and is necessary for their targeted secretion to this domain
572 (Kalmbach et al. 2017). Accordingly, *exo70a1* mutants display a high
573 number of non-localized and non-functional, unstable CASP microdomains.
574 What mechanism could account for the selective stabilization of CASPs in
575 domains facing intact neighbors of the same differentiation state, but not
576 towards dead, undifferentiated cells or cells of a different cellular identity?
577 One explanation would postulate the existence of a stabilizing short-range
578 signal, produced by CASPs domain that can only act *in trans*, not *in cis*.
579 However, such an exclusive *in trans* action is difficult to conceive with
580 small, released molecules able to diffuse across the cell wall space. It would
581 be much easier to conceive with filaments, reaching across the cell walls
582 between domains, but there is no evidence for the existence of such
583 filament-like structures. Alternatively, a cumulative threshold for a short-
584 range, stabilizing signal produced by the microdomains can be postulated,
585 that could only be reached when both cells produce it. However, such a
586 model would require a very fine-tuned thresholding. Although a promising
587 candidate for a factor involved in this coordination process, our detailed
588 analysis of the *lotr1* mutant demonstrates that it does not affect the
589 coordination of the properly localized micro-domains between cells, nor
590 does it allow for their formation without neighbors. Nevertheless, absence

591 of LOTR1 activity clearly allows for formation of non-paired, stable, and
592 fully functional microdomains, oriented towards non-endodermal
593 neighbors. Therefore, it is most likely responsible for inhibiting sporadic
594 micro-domain formation throughout the endodermal membrane when
595 CASPs are starting to focalize from their ubiquitous distribution in the
596 plasma membrane into aligned micro-domains. The peculiar formation of
597 Casparian half-strips in *lotr1*, further indicates that lignin deposition into
598 the CS cell wall is separately performed by both contributing cells, which
599 would make a tight coordination of neighboring CASP domains all the more
600 critical for achieving a fully sealed cell wall space. Restricted mostly to the
601 stele in mature regions of the root, we provide evidence that this putative
602 cell wall protease might act on a target originating outside of its own
603 expression profile. *lotr1* could only be complemented using stele-specific
604 promoters and neither endodermal, cortex nor ubiquitous expression leads
605 to complementation. Importantly we discovered that wildtype plants
606 displayed a dominant *lotr1*-like phenotype with ectopic patches, disrupted
607 CSDs, and a corresponding delay in PI block when LOTR1 was mis-
608 expressed in the cortex. How could ectopic expression of a putative cell
609 wall protease in the cortex interfere with the action of the same protease
610 in its wild-type expression domain in the stele? The most parsimonious
611 explanation we can conceive is that a LOTR1 substrate is produced in the
612 outer cortical tissues and has to diffuse into the stele for activation by
613 stele-expressed LOTR1 (Fig. 6). Expression of LOTR1 in the cortex would
614 lead to a premature activation of its substrate in the cortex and not allow it
615 to reach the stele. It would thus deplete the endogenous LOTR1 of its
616 substrate and cause the observed dominant loss-of-function phenotype.
617 This explanation thus draws a "reverse" SGN3/CIF pathway model where a
618 cortex-specific substrate passes across the endodermal cell layer to be
619 activated by a stele-specific enzyme complex, destabilizing CASPs and
620 preventing domain formation at ectopic positions.

621

622 **Acknowledgments**

623 We wish to thank the Central Imaging Facility (CIF) and the Electron
624 Microscopy Facility (EMF) of the University of Lausanne for their technical
625 expertise. We thank Baohai Li and Takehiro Kamiya (Tokyo University) for
626 initial discussions on the project and exchange of material. We also thank
627 Hiroko Uchida and Marie Barberon for their graphical work. This work was
628 supported by an ERC Consolidator Grant (GA-N°: 616228—ENDOFUN) and
629 two SNSF grants (CRSII3_136278 and 31003A_156261) to N.G., and a
630 Federation of European Biochemical Sciences Postdoctoral Long-Term
631 Fellowship to P.M..

632 **Author contributions**

633 AK, PM, LK, and NG conceived and designed the project. AK, PM, and DDB
634 performed experiments and AK and PM performed image quantification.
635 AK and NG wrote the manuscript and all authors revised the manuscript.

636

637 **Declaration of Interests**

638 The authors declare that they have no conflict of interest.

639 **Figure legends**

640 **Fig. 1: Ectopic domain formation in *lotr1.***

641 A Schematic representation of endodermal maturation with stages of
642 Casparian Strip (CS) development (green). Elongated endodermal cells
643 focalize CASP1-GFP into aligned micro-domains which are subsequently
644 fused into a continuous ring around each endodermal cells.

645 B CASP1-GFP localization in wildtype and *lotr1* with focus on patch
646 localization. Images depict maximum intensity projections of z-stack
647 images. 3D reconstruction image depicts region indicated in *lotr1* overview
648 image, section view images are annotated by yellow (top) and blue
649 (bottom) arrows. Overview images scale bars: 20 µm; 3D reconstruction &
650 section views scale bars: 10 µm.

651 C 3D schematic for visualization of median endodermal cell section with
652 annotated cell faces.

653 D TEM section of *lotr1* obtained at 2 mm from root tip. Overview of section
654 with focus on regular CS and adjacent ectopic patch. Closeup indicated by
655 dashed black line in overview image; en = endodermis, pe = pericycle, co =
656 cortex, scale bars = 2 µm.

657 E Consecutive TEM sections at 2 mm from root tip, with and without
658 $KMnO_4$ staining, position indicated in (D). Dark deposits indicate electron-
659 dense MnO_2 precipitation caused by reaction with lignin. Note that in the
660 case of ectopic patches, the staining is restricted to the endodermal side of
661 the cell wall; en = endodermis, pe = pericycle, interspaced white line
662 depicts extend of CS-like cell wall morphology, scale bar = 1 µm.

663 F Localization of enzymes necessary for CS lignification in wildtype Col-0
664 and *lotr1*, pictures depict cells as seen in (C). Cellulosic cell walls are stained
665 with Calcofluor White and depicted in white in overlay images, scale bar =
666 10 µm.

667

668 **Fig. 2: CASP deposition is coordinated between neighboring endodermal**
669 **cells.**

670 A Double membrane phenotype visible with CASP1::CASP1-GFP during
671 string-of-pearls stage of CS development, scale bars depict 10 µm. Red and
672 grey arrows indicate separate membranes measured in (B).

673 B Comparison of GFP intensity between adjacent membranes indicated in
674 (A). Pixel intensity was measured along each membrane and relative GFP
675 intensity was adjusted to mean intensity of each membrane. Correlation of

676 original intensities (R-squared) was determined by fitting of a linear model
677 with indicated probability of fit (p-value).

678 C Localization of CSD marker CASP1-GFP in comparison to cell wall protein
679 ESB1-mCherry at early and mature CSs, scale bar depicts 5 µm.

680 D,E Double membrane phenotype of CASP1-GFP before and after ablation
681 of one adjacent endodermal cell in early (D) and late (E) CSs. Cell walls (red)
682 are stained with Propidium iodide (PI), yellow arrows indicate intensity
683 profiles measured in F-I; asterisks indicate ablated cell, scale bars = 5 µM.

684 F-I Quantification of CASP1-GFP and PI intensity before and after cell
685 ablation. Intensity was quantified in a 7-pixel wide line indicated in (D) and
686 (E).

687

688 **Fig. 3: Endodermal neighbors are required for proper CSD establishment**

689 A Endodermal cell ablation leads to instability of the CSD in membranes
690 facing dead cells. Endodermal cells were ablated 3-5 cells prior to onset of
691 CASP1-GFP (white) expression and followed over indicated time spans. First
692 image depicts overview after ablation with cells outlined with PI; # depicts
693 remaining live endodermal cell, dashed yellow line depicts cell outlines of
694 ablated cells, arrow indicates onset of CASP expression, dashed green and
695 red rectangles indicate quantification areas shown in (B), scale bar = 20
696 µm.

697 B Quantification of GFP fluorescence over time in membranes facing live
698 (green) and dead (red) adjacent endodermal cells. Intensity depicted in
699 relation to maximum total GFP intensity.

700 C Ablation of all adjacent endodermal cells prevents fusion of CSDs.
701 Endodermal neighbors were ablated at timepoint 0 and CASP1-GFP
702 expression (white) followed over time in remaining cell (#), PI (red)
703 highlighted cell outlines and confirmed destruction of cells; yellow arrow
704 indicates initial CASP microdomains, scale bar = 50 um.

705 D CASP instability in membranes facing ablated cells is independent from
706 CASP expression. Cells ablated 3-5 cells prior to onset of CASP expression,
707 cell outline depicted with dashed yellow line, arrow indicates stable CASP
708 formation, scale bar = 100 um.

709 E CASP fusion occurs only if both neighboring cells reach expression
710 threshold. Endodermal differentiation was induced via 0.5 µM β-estradiol
711 and CASP1-GFP expression followed over the next 12 h. Yellow arrows
712 indicate CASP deposits in the membrane, dashed green and red rectangles
713 indicate areas for quantification shown in (F).

714 F Quantification of GFP fluorescence over time in membranes reaching
715 local stability threshold (green) and those below the threshold (red).

716

717 **Fig. 4: LOTR1 restricts CSD establishment through independent pathway.**

718 A CASP1-GFP fluorescence of known CS mutants in wildtype and *lotr1*
719 background. Yellow arrows indicate parental CS mutant phenotype while
720 blue arrows highlight *lotr1* specific phenotypes; scale bar = 20 um.

721 B Enhanced lignification in *lotr1* is SCHENGEN-dependent. Ectopic lignin
722 (magenta) accumulates in *lotr1* at disruptions of the CASP1-GFP (green)
723 marked CSD. Lignification of the central domain and ectopic patches is
724 unaffected by disruption of *SGN3*, scale bar = 20 um.

725 C Apoplastic barrier phenotypes of *lotr1* double mutants. Formation of
726 apoplastic barrier was determined by penetrance of apoplastic tracer PI to
727 the stele; n = 10, significance determined by one-way ANOVA and separate
728 groups identified with Tukey-Kramer test.

729 D SCHENGEN-pathway is unaffected in *lotr1*. Wildtype and *lotr1* seedlings
730 were treated for 24 h with 100 µM synthetic CIF2 peptide and lignin
731 accumulation (magenta) outside the regular CSD domain (green) analysed.
732 Cell walls were stained with Calcofluor White, yellow arrows indicate
733 ectopic lignin accumulation, scale bar = 5 µm.

734 E LOTR1 expression indicates additional roles. Promoter activity highlighted
735 by tdTomato fluorescence in 5 day old seedlings; cells outlined by
736 Propidium iodide (white); mid-view regions depicted below highlighted by
737 continuous rectangles (a,b) and section views indicated by dash-dotted
738 lines (c,d), inlay shows colour profile of *LOTR1* expression intensity. a
739 Single-plane section through root meristem region, arrow indicates cortex-
740 daughter cell. b Single-plane section after cell elongation, arrows indicate
741 expression in endodermis (top arrow) and epidermis (bottom arrow). c
742 Maximum-intensity projection of section view of z-stack through meristem
743 region indicated in top picture. d Maximum-intensity projection of section
744 view of z-stack through mature region indicated in top picture; * denotes
745 endodermal cell lineage, scale bars: *top*: 100 um; *a*,*b*: 20 um; *c*,*d*: 50 um.

746 F Phylogenetic analysis of *HOMOLOGS-OF-LOTR1* (HOLO) family in
747 *Arabidopsis thaliana*. Homologs of LOTR1 in *A.thaliana* were identified and
748 grouped into five subfamilies by phylogenetic distance, LOTR1 (At5g50150)
749 highlighted in red, underlined genes have predicted N-terminal
750 transmembrane domains.

751 **Fig. 5: Stele-specific LOTR1 is restricts CSD establishment through a**
752 **cortex-expressed, mobile target.**

753 A Complementation of *lotr1* phenotype. N-terminal fusion construct
754 expressed under native *LOTR1* promoter complements ectopic CSD
755 phenotype. Scale bars: *left* 100 um, *section views* 20 um.

756 B Overexpression of *LOTR1* in wild-type and *lotr1* backgrounds does not
757 affect complementation. CASP1-GFP phenotype of seedlings grown for 5
758 days on control or 5 µM β-estradiol; scale bar: 20 um.

759 C Mis-expression of LOTR1 in cortical cells causes dominant loss-of-
760 function phenotypes. CASP1-GFP phenotypes of seedlings expressing
761 LOTR1-complementation construct used in (A) under indicated promoters.
762 Activity of used promoter indicated in schematics below; blue arrows
763 indicate *lotr1*-like phenotypes; EP = epidermis, CO = cortex, EN =
764 endodermis, ST = stele; scale bars = 20 um.

765 D Apoplastic barrier phenotypes of tissue specific complementation lines in
766 wildtype (white) and *lotr1* (grey) background. Cells after onset of
767 elongation counted until penetrance of PI was blocked. n = 10, significance
768 determined via one-way ANOVA and independent groups identified via
769 Tukey-Kramer post-hoc test.

770 **Fig. 6: Speculative model of LOTR1 function**

771 **Wild-type:** LOTR1 is a predicted protease (*scissors*), experimentally
772 determined to be expressed in the stele and to localize in the cell wall. We
773 speculate that LOTR1 cleaves a cortex-derived substrate (*grey, dark-red*
774 *coffee bean*, *inactive*), activating it in the stele (*red half-bean, active*). This
775 substrate then inhibits ectopic CASP-domain formation (*green*) at the stele-
776 facing endodermal surface by unknown means. **lotr1 mutant:** Absence of
777 LOTR1 would not allow activation of the ectopic CASP-domain inhibitor in
778 the endodermal, stele-facing apoplast, leading to the observed formation
779 of ectopic, stable CASP-domain predominantly at the stele-facing side of
780 the endodermal surface. **LOTR1 cortex mis-expression:** This model explains
781 the observation that cortical mis-expression of LOTR1 dominantly
782 interferes with wild-type LOTR1 action, if it would precociously cleave and
783 activate the LOTR1 substrate, not allowing it to reach the stele to be
784 activated by wild-type LOTR1. This would lead to the observed, similar
785 phenotype than the lotr1 knock-out.

786

787

788 **STAR Methods**

789 *Plant material and growth conditions*

790 All experiments were performed in the *Arabidopsis thaliana* Columbia-0
791 ecotype. T-DNA insertion lines obtained from NASC: *lotr1-10*
792 (SALK_051707) (Li et al. 2017), *sgn3-3* (SALK_043282) (Pfister et al. 2014),
793 *sgn1-2* (SALK_055095C) (J Alassimone et al. 2016), *sgn2-2* (SALK_009847)
794 (Doblas et al. 2017); *myb36-2* (GK- 543B11) (Kamiya et al. 2015), *esb1-1*
795 was kindly shared by Prof. David Salt's group (Hosmani et al. 2013), and the
796 *lotr1-1* allele was identified in the *LOTR*-screen (Li et al. 2017). Inducible
797 pUBQ10>>XVE::MYB36 were obtained from the TRANSPLANTA collection
798 (N2102512 and N2102513) and crossed to CASP1::CASP1-GFP. If not
799 otherwise stated, plants were grown as follows: Seeds were surface
800 sterilized and sown on half-strength Murashige-Skoog medium (Duchefa)
801 solidified with 0.8 % plant agar (Duchefa). After stratification for 2 days at 4
802 °C, seeds were germinated in growth chambers with long-day conditions
803 (16 h light/8 h dark) and temperature cycling between 22 °C/19 °C
804 (day/night). 5 days after germination, seedlings were directly analysed or
805 cleared and stained with ClearSee as described (Ursache et al. 2018). For
806 long-term imaging, agar blocks with seedlings were cut and transferred
807 into microscope chamber slides (Marhavý and Benková 2015; Marhavý et
808 al. 2016) and equal volume of double-concentrated β-estradiol added
809 before imaging.

810 *Plasmid construction*

811 A 3 kb promoter fragment of *LOTR1* was generated by 5'-
812 aacaggtctcgacctctttctatctgtttgtacctaagt-3' and 5'-
813 aacaggtctcatgttaactagagaatgtacggcttgttt-3' and cloned via Eco31I-
814 restriction sites into GreenGate entry module vector pGGA000
815 (Lampropoulos et al. 2013). Genomic fragment of *LOTR1* coding sequence
816 was amplified with 5'-
817 aacaggtctcaggctcgatgTCAGCTATTCATCTTAAAAACCAAACTTCA and 5'-
818 aacaggtctcaCTGAAGGACACCTTGGGTTCCG-3' and cloned into pGGC000.
819 mScarlet-I was amplified from pmScarlet-I_C1 (Bindels et al. 2016)

820 obtained from Addgene and secretion peptide was added by tandem PCR
821 amplification with 5'-
822 gctctttccctctatctcctgcccaatccagccactagtATGGTGAGCAAGGGCGAG-3' (FW1)
823 and 5'-
824 aacaGGTCTCaAACAatgaaagccttcacactcgctctcttcttagctctttccctctatctcctg-3'
825 (FW2) and 5'-aacaGGTCTCaAGCCCTTGTACAGCTCGTCCATGC-3' (RV) and
826 cloned via Eco31I sites into pGGB000. Final destination clones were
827 obtained by subsequent GoldenGate reaction with pGreenII based
828 pGGZ003 and transformed into *Arabidopsis* using floral dip.

829 *Confocal imaging*

830 Imaging was performed on Leica SP8 or Zeiss LSM880 microscopes,
831 excitation and emission as follows (excitation, detection): Calcofluor White
832 (405 nm, 425 – 475 nm), GFP (488nm, 500 – 550 nm),
833 mCherry/tdTomato/mScarlet-I (563 nm, 580 – 650 nm), PI (563 nm, 580 –
834 650 nm), basic Fuchsin (563 nm, 580 – 650 nm).

835 *PI assay*

836 PI was performed as described in Lee et al. 2013 with following changes:
837 Seedlings were incubated in 10 µg/ml PI dissolved in water for 5 min and
838 imaged immediately afterwards. Number of endodermal cells determined
839 after onset of elongation (defined as first endodermal cell with length to
840 width ratio of at least 2, i.e. at least twice as long than wide).

841 *Transmission electron microscopy (TEM)*

842 5-day-old Arabidopsis seedlings were fixed in glutaraldehyde solution
843 (EMS, Hatfield, PA) 2.5% in 100 mM phosphate buffer (pH 7.4) for 1 hour at
844 room temperature. Then, they were post-fixed in osmium tetroxide 1%
845 (EMS) with 1.5% of potassium ferrocyanide (Sigma, St. Louis, MO) in
846 phosphate buffer for 1 hour at room temperature. Following that, the
847 plants were rinsed twice in distilled water and dehydrated in ethanol
848 solution (Sigma) at gradient concentrations (30% 40 min; 50% 40 min; 70%
849 40 min; two times (100% 1 hour). This was followed by infiltration in Spurr
850 resin (EMS) at gradient concentrations (Spurr 33% in ethanol, 4 hours;

851 Spurr 66% in ethanol, 4 hours; Spurr two times (100% 8 hours) and finally
852 polymerized for 48 hours at 60°C in an oven. Ultrathin sections 50 nm thick
853 were cut transversally at 2mm ± 0.2 mm from the root tip, on a Leica
854 Ultracut (Leica Mikrosysteme GmbH, Vienna, Austria) and two consecutive
855 sections were picked up on a nickel slot grid 2X1 mm (EMS) coated with a
856 polystyrene film (Sigma).

857 *Lignin staining with permanganate potassium ($KMnO_4$) using TEM*

858 Visualization of lignin deposition around Casparian strip was done using
859 permanganate potassium ($KMnO_4$) staining (Hepler, Fosket, and Newcomb
860 1970). The first section was imaged without any post-staining. Then the
861 sections were post-stained using 1% of $KMnO_4$ in H_2O (Sigma, St Louis, MO,
862 US) for 45min and rinsed several times with H_2O. Then the second section
863 of the grid was imaged. Micrographs were taken with a transmission
864 electron microscope FEI CM100 (FEI, Eindhoven, The Netherlands) at an
865 acceleration voltage of 80kV and 11000X magnifications (pixel size of
866 1.851nm), with a TVIPS TemCamF416 digital camera (TVIPS GmbH,
867 Gauting, Germany) using the software EM-MENU 4.0 (TVIPS GmbH,
868 Gauting, Germany). Panoramic were aligned with the software IMOD
869 (Kremer, Mastronarde, and McIntosh 1996).

870 *Cell ablation*

871 Endodermal cells were ablated using a MaiTai-SpectraPhysics laser at 800
872 nm integrated into a Zeiss LSM880 microscope. A ROI outlining the cells to
873 ablate was used and cells were ablated with 2 % power and 0.8 µs pixel
874 dwell time. Cell destruction was confirmed using transmitted light and PI
875 staining.

876 *Western blot*

877 Roots of 5-day old seedlings grown on ½ MS medium were cut and
878 weighted before shock-freezing in liquid nitrogen. Samples were then
879 homogenized using TissueLyser II (Qiagen). Proteins were then denatured
880 by addition of 3x (v/w) 1x NuPAGE LDS sample buffer + 50 mM DTT
881 (Invitrogen, NP0007) and heating for 5 min at 70 °C. Cell debris was

882 removed by centrifugation at 1'000 *g* for 5 min before separation of
883 proteins on pre-cast 12 % Bis-Tris SDS-PAGE gels (iD PAGE, Eurogentec).
884 After electrophoresis, proteins were transferred onto PVDF membrane
885 using Pierce FastBlotter G2 semi-dry blotting. Membranes were then
886 blocked (5 % skim milk in TBS) for 1 h before incubation with anti-RFP
887 antibody (1:1000, Chromotek 6G6) overnight at 4 °C. After washing the
888 membrane three times with 1x TBS + 0.1 % Tween (TBS-T), blot incubated
889 for 2 h at root temperature with anti-mouse-HRP antibody (1:5000).
890 Finally, after washing blot three times with TBS-T, HRP activity was
891 detected using SuperSignal West Femto Kit (Thermo Scientific) and GE
892 ImageQuant LAS 500.

893 *Phylogenetic analysis*

894 Homologs of LOTR1 were identified by searching the *Arabidopsis thaliana*
895 proteome for proteins containing both Neprosin-AP (PF14365) and
896 Neprosin domains (PF03080). Sequence similarity was compared using
897 MUSCLE (EMBL-EBI, Madeira et al. 2019). Phyolgenetic analysis was done
898 using the NGPhylogeny.fr online-tool with PhylML+SMS settings. Final tree
899 was assembled and annotated with iTOL online tool (Letunic and Bork
900 2019). Conserved residues were identified using pre-aligned sequences and
901 the online-weblogo tool from the University of Berkely
902 (https://weblogo.berkeley.edu/logo.cgi) (Crooks et al. 2004).

903 *Statistical analysis*

904 Statistical analysis was done in R software (R Core Team, 2013)
905 (https://www.r-project.org/). For multiple group comparisons, one-way
906 ANOVA was performed, and significantly different groups identified with
907 Tukey-Kramer post-hoc test.

908

909 **Fig. S1: Establishment of ectopic domain formations in *lotr1*.**

910 A Localization of ectopic deposition of CASP1-GFP (green). Section view of
911 z-stack through roots 5-10 cells after onset of protoxylem differentiation,
912 cell wall stained with Calcofluor White (white) and crops shown on top
913 outlined in overview pictures below (dashed yellow line); scale bar = 50
914 um, c = cortex, e = endodermis, p = pericycle.

915 B Quantification of ectopic CASP1-GFP patches. Number and position of
916 ectopic patches were determined per cell and depicted as ratio of patches
917 facing pericycle cells vs total patch number, maximum of 3 cells counted
918 per seedling, n_{total} = 11.

919 C Deposition of CASP1-GFP in *lotr1*. CASP1-GFP fluorescence depicted
920 throughout CSD formation in *lotr1*; scale bars = 5 um. Kymograph image at
921 bottom illustrates fluorescence over time in line indicated above, individual
922 patch formation visible as independent pyramid-like structures (yellow
923 arrows).

924 D TEM section of wildtype at 2 mm. Closeup indicated by dashed black line
925 in overview image, en = endodermis, pe = pericycle, scale bars = 2 µm.

926 E Consecutive TEM sections at 2 mm from root tip, with and without
927 $KMnO_4$ staining. Dark deposits indicate electron-dense MnO_2 precipitation
928 caused by reaction with lignin; en = endodermis, pe = pericycle, black
929 arrows indicate CS-like cell wall with attached plasma membranes, white
930 arrows highlight plasmolyzed membranes detached from the cell wall,
931 scale bar = 1 µm.

932

933 **Fig. S2: CASP1-GFP membrane coordination.**
934 Double membrane phenotype in CS mutants, scale bars = 5 um. R^2 value
935 depicts Spearman rho correlation coefficients of fluorescence of 5 pixel
936 wide lines following each membrane.

937

938 **Fig. S3: Cell ablation impacts CS establishment.**
939 A CASP1 promoter activity highlighted by nls-GFP (green) after ablation of
940 all neighboring cells prior to onset of expression, PI (red) outlines cells and
941 confirmed cell destruction. Scale bar = 50 um.

942 B Endodermal differentiation was induced via 0.5 µM β-estradiol and
943 CASP1-GFP expression (white) followed over the next 12 h. Red arrows
944 indicate unstable CASP deposits in the membrane, scale bar = 50 um.

945 C CSD formation in wildtype and *lotr1*. Single endodermal cells ablated 3-4
946 cells prior to onset of CASP expression, * depicts ablated cell, scale bar = 50
947 um.

948

949 **Fig. S4: Investigation of putative post-translational processing in LOTR1.**

950 A Lignin accumulation (magenta) in wildtype and *sgn3* with CSDs labelled
951 by CASP1-GFP (green).

952 B Schematic view of LOTR1 with position of identified loss-of-function
953 alleles indicated.

954 C Processing of LOTR1. Root protein extracts separated via SDS-PAGE and
955 LOTR1-fragments detected by anti-RFP antibody (Chromotek 6G6). Note
956 that C-terminal fusion construct LOTR1::LOTR1-mCherry does not
957 complement the *lotr1* phenotype, but shows processing/degradation
958 fragments. Both weak (#1) and strong (#2) C-terminal complementation
959 lines lack processing/degradation fragments.

960 D Complementation analysis of the *lotr1* CASP1-GFP phenotype using
961 truncated versions consisting of only LOTR1's Neprosin domain (Neprosin),
962 the putative autoinhibitory Neprosin-AP domain (Neprosin-AP), or full-
963 length LOTR1 with conserved cysteines C255 and C260 mutated
964 ($LOTR1^{C255A, C260A}$), scale bars = 50 µm.

965

966 **Fig. S5: Neprosin domain analysis in the HOLO family.**
967 A Conservation of Neprosin domain throughout the HOLO-family, including
968 LOTR1. Putative catalytic triade amino acids aligning with *E.coli* mepS
969 marked with red arrows.

970 B Sequence alignment of *E.coli* mepS, Neprosin, LOTR1 and its closest
971 homologs At1g23340 (HOLO2), At1g70550 (HOLO3), and At1g10750
972 (HOLO4)

973

974

975 **References**

976 Alassimone, J, S Fujita, V G Doblas, M van Dop, M Barberon, L Kalmbach, J E
977 Vermeer, et al. 2016. "Polarly Localized Kinase SGN1 Is Required for
978 Casparian Strip Integrity and Positioning." *Nat Plants* 2: 16113.
979 https://doi.org/10.1038/nplants.2016.113.

980 Alassimone, Julien, Sadaf Naseer, and Niko Geldner. 2010. "A
981 Developmental Framework for Endodermal Differentiation and
982 Polarity." *Proc Natl Acad Sci U S A* 107 (11): 5214–19.
983 https://doi.org/10.1073/pnas.0910772107.

984 Bao, Zhulatai, Juan Bai, Hongchang Cui, and Chunmei Gong. 2019. "A
985 Missing Link in Radial Ion Transport: Ion Transporters in the
986 Endodermis." *Frontiers in Plant Science* 10 (June): 1–8.
987 https://doi.org/10.3389/fpls.2019.00713.

988 Barbosa, Inês Catarina Ramos, Nelson Rojas-Murcia, and Niko Geldner.
989 2019. "The Casparian Strip—One Ring to Bring Cell Biology to
990 Lignification?" *Current Opinion in Biotechnology* 56: 121–29.
991 https://doi.org/10.1016/j.copbio.2018.10.004.

992 Bindels, Daphne S., Lindsay Haarbosch, Laura Van Weeren, Marten Postma,
993 Katrin E. Wiese, Marieke Mastop, Sylvain Aumonier, et al. 2016.
994 "MScarlet: A Bright Monomeric Red Fluorescent Protein for Cellular
995 Imaging." *Nature Methods*. https://doi.org/10.1038/nmeth.4074.

996 Crooks, Gavin E, Gary Hon, John Marc Chandonia, and Steven E. Brenner.
997 2004. "WebLogo: A Sequence Logo Generator." *Genome Research* 14
998 (6): 1188–90. https://doi.org/10.1101/gr.849004.

999 Denyer, Tom, Xiaoli Ma, Simon Klesen, Emanuele Scacchi, Kay Nieselt, and
1000 Marja C.P. Timmermans. 2019. "Spatiotemporal Developmental
1001 Trajectories in the Arabidopsis Root Revealed Using High-Throughput
1002 Single-Cell RNA Sequencing." *Developmental Cell* 48 (6): 840-852.e5.
1003 https://doi.org/10.1016/j.devcel.2019.02.022.

1004 Doblas, Verónica G, Elwira Smakowska-Luzan, Satoshi Fujita, Julien

1005 Alassimone, Marie Barberon, Mathias Madalinski, Youssef Belkhadir,
1006 and Niko Geldner. 2017. "Root Diffusion Barrier Control by a
1007 Vasculature-Derived Peptide Binding to the SGN3 Receptor." *Science*
1008 355 (6322): 280–84. https://doi.org/10.1126/science.aaj1562.

1009 Enstone, Daryl E., Carol A. Peterson, and Fengshan Ma. 2002. "Root
1010 Endodermis and Exodermis: Structure, Function, and Responses to the
1011 Environment." *Journal of Plant Growth Regulation*. Springer.
1012 https://doi.org/10.1007/s00344-003-0002-2.

1013 Fujita, Satoshi, Damien De Bellis, Kai H Edel, Philipp Köster, Tonni Grube
1014 Andersen, Emanuel Schmid-Siegert, Valérie Dénervaud Tendon, et al.
1015 2020. "SCHENGEN Receptor Module Drives Localized ROS Production
1016 and Lignification in Plant Roots." *The EMBO Journal*, e103894.
1017 https://doi.org/10.15252/embj.2019103894.

1018 Geldner, Niko. 2013. "The Endodermis." *Annual Review of Plant Biology* 64
1019 (1): 531–58. https://doi.org/10.1146/annurev-arplant-050312-
1020 120050.

1021 Hepler, Peter K., Donald E. Fosket, and Eldon H. Newcomb. 1970.
1022 "LIGNIFICATION DURING SECONDARY WALL FORMATION IN COLEUS:
1023 AN ELECTRON MICROSCOPIC STUDY." *American Journal of Botany* 57
1024 (1): 85–96. https://doi.org/10.1002/j.1537-2197.1970.tb09793.x.

1025 Hosmani, P S, T Kamiya, J Danku, S Naseer, N Geldner, M L Guerinot, and D
1026 E Salt. 2013. "Dirigent Domain-Containing Protein Is Part of the
1027 Machinery Required for Formation of the Lignin-Based Casparian Strip
1028 in the Root." *Proc Natl Acad Sci U S A* 110 (35): 14498–503.
1029 https://doi.org/10.1073/pnas.1308412110.

1030 Itoh, Masahiko, and Mina J. Bissell. 2003. "The Organization of Tight
1031 Junctions in Epithelia: Implications for Mammary Gland Biology and
1032 Breast Tumorigenesis." *Journal of Mammary Gland Biology and*
1033 *Neoplasia* 8 (4): 449–62.
1034 https://doi.org/10.1023/B:JOMG.0000017431.45314.07.

1035 Kalmbach, L, K Hematy, D De Bellis, M Barberon, S Fujita, R Ursache, J
1036 Daraspe, and N Geldner. 2017. "Transient Cell-Specific EXO70A1
1037 Activity in the CASP Domain and Casparian Strip Localization." *Nat*
1038 *Plants* 3: 17058. https://doi.org/10.1038/nplants.2017.58.

1039 Kamiya, Takehiro, Monica Borghi, Peng Wang, John M. C. Danku, Lothar
1040 Kalmbach, Prashant S. Hosmani, Sadaf Naseer, Toru Fujiwara, Niko
1041 Geldner, and David E. Salt. 2015. "The MYB36 Transcription Factor
1042 Orchestrates Casparian Strip Formation." *Proc Natl Acad Sci U S A* 112
1043 (33): 10533–38. https://doi.org/10.1073/pnas.1507691112.

1044 Kremer, James R, David N Mastronarde, and J.Richard McIntosh. 1996.
1045 "Computer Visualization of Three-Dimensional Image Data Using
1046 IMOD." *Journal of Structural Biology* 116 (1): 71–76.
1047 https://doi.org/10.1006/jsbi.1996.0013.

1048 Lampropoulos, A, Z Sutikovic, C Wenzl, I Maegele, J U Lohmann, and J
1049 Forner. 2013. "GreenGate---a Novel, Versatile, and Efficient Cloning
1050 System for Plant Transgenesis." *PLoS One* 8 (12): e83043.
1051 https://doi.org/10.1371/journal.pone.0083043.

1052 Lee, Y, M C Rubio, J Alassimone, and N Geldner. 2013. "A Mechanism for
1053 Localized Lignin Deposition in the Endodermis." *Cell* 153 (2): 402–12.
1054 https://doi.org/10.1016/j.cell.2013.02.045.

1055 Letunic, Ivica, and Peer Bork. 2019. "Interactive Tree of Life (ITOL) v4:
1056 Recent Updates and New Developments." *Nucleic Acids Research*.
1057 https://doi.org/10.1093/nar/gkz239.

1058 Li, B, T Kamiya, L Kalmbach, M Yamagami, K Yamaguchi, S Shigenobu, S
1059 Sawa, et al. 2017. "Role of LOTR1 in Nutrient Transport through
1060 Organization of Spatial Distribution of Root Endodermal Barriers." *Curr*
1061 *Biol* 27 (5): 758–65. https://doi.org/10.1016/j.cub.2017.01.030.

1062 Liberman, L M, E E Sparks, M A Moreno-Risueno, J J Petricka, and P N
1063 Benfey. 2015. "MYB36 Regulates the Transition from Proliferation to
1064 Differentiation in the Arabidopsis Root." *Proc Natl Acad Sci U S A* 112

1065 (39): 12099–104. https://doi.org/10.1073/pnas.1515576112.

1066 Ma, Jian Feng, Naoki Yamaji, Namiki Mitani, Kazunori Tamai, Saeko Konishi,
1067 Toru Fujiwara, Maki Katsuhara, and Masahiro Yano. 2007. "An Efflux
1068 Transporter of Silicon in Rice." *Nature*.
1069 https://doi.org/10.1038/nature05964.

1070 Madeira, Fábio, Young Mi Park, Joon Lee, Nicola Buso, Tamer Gur, Nandana
1071 Madhusoodanan, Prasad Basutkar, et al. 2019. "The EMBL-EBI Search
1072 and Sequence Analysis Tools APIs in 2019." *Nucleic Acids Research*.
1073 https://doi.org/10.1093/nar/gkz268.

1074 Marhavý, Peter, and Eva Benková. 2015. "Real-Time Analysis of Lateral
1075 Root Organogenesis in Arabidopsis." *BIO-PROTOCOL* 5 (8).
1076 https://doi.org/10.21769/BioProtoc.1446.

1077 Marhavý, Peter, Juan Carlos Montesinos, Anas Abuzeineh, Daniel Van
1078 Damme, Joop E.M. Vermeer, Jerôme Duclercq, Hana Rakusová, et al.
1079 2016. "Targeted Cell Elimination Reveals an Auxin-Guided Biphasic
1080 Mode of Lateral Root Initiation." *Genes and Development* 30 (4): 471–
1081 83. https://doi.org/10.1101/gad.276964.115.

1082 Nakayama, Takuya, Hidefumi Shinohara, Mina Tanaka, Koki Baba, Mari
1083 Ogawa-Ohnishi, and Yoshikatsu Matsubayashi. 2017. "A Peptide
1084 Hormone Required for Casparian Strip Diffusion Barrier Formation in
1085 Arabidopsis Roots." *Science* 355 (6322): 284–86.
1086 https://doi.org/10.1126/science.aai9057.

1087 Naseer, S, Y Lee, C Lapierre, R Franke, C Nawrath, and N Geldner. 2012.
1088 "Casparian Strip Diffusion Barrier in Arabidopsis Is Made of a Lignin
1089 Polymer without Suberin." *Proc Natl Acad Sci U S A* 109 (25): 10101–6.
1090 https://doi.org/10.1073/pnas.1205726109.

1091 Pfister, A, M Barberon, J Alassimone, L Kalmbach, Y Lee, J E Vermeer, M
1092 Yamazaki, et al. 2014. "A Receptor-like Kinase Mutant with Absent
1093 Endodermal Diffusion Barrier Displays Selective Nutrient Homeostasis
1094 Defects." *Elife* 3: e03115. https://doi.org/10.7554/eLife.03115.

1095 Rajasekaran, Ayyappan K., Minoru Hojo, Tellervo Huima, and Enrique
1096 Rodriguez-Boulan. 1996. "Catenins and Zonula Occludens-1 Form a
1097 Complex during Early Stages in the Assembly of Tight Junctions."
1098 *Journal of Cell Biology* 132 (3): 451–63.
1099 https://doi.org/10.1083/jcb.132.3.451.

1100 Rey, M, M Yang, L Lee, Y Zhang, J G Sheff, C W Sensen, H Mrazek, et al.
1101 2016. "Addressing Proteolytic Efficiency in Enzymatic Degradation
1102 Therapy for Celiac Disease." *Sci Rep* 6: 30980.
1103 https://doi.org/10.1038/srep30980.

1104 Roppolo, Daniele, Bert De Rybel, Valérie Dénervaud Tendon, Alexandre
1105 Pfister, Julien Alassimone, Joop E. M. Vermeer, Misako Yamazaki,
1106 York-Dieter Stierhof, Tom Beeckman, and Niko Geldner. 2011. "A
1107 Novel Protein Family Mediates Casparian Strip Formation in the
1108 Endodermis." *Nature* 473 (7347): 380–83.
1109 https://doi.org/10.1038/nature10070.

1110 Ryu, K H, L Huang, H M Kang, and J Schiefelbein. 2019. "Single-Cell RNA
1111 Sequencing Resolves Molecular Relationships Among Individual Plant
1112 Cells." *Plant Physiol* 179 (4): 1444–56.
1113 https://doi.org/10.1104/pp.18.01482.

1114 Schrader, C U, L Lee, M Rey, V Sarpe, P Man, S Sharma, V Zabrouskov, B
1115 Larsen, and D C Schriemer. 2017. "Neprosin, a Selective Prolyl
1116 Endoprotease for Bottom-up Proteomics and Histone Mapping." *Mol*
1117 *Cell Proteomics* 16 (6): 1162–71.
1118 https://doi.org/10.1074/mcp.M116.066803.

1119 Siligato, R, X Wang, S R Yadav, S Lehesranta, G Ma, R Ursache, I Sevilem, et
1120 al. 2016. "MultiSite Gateway-Compatible Cell Type-Specific Gene-
1121 Inducible System for Plants." *Plant Physiol* 170 (2): 627–41.
1122 https://doi.org/10.1104/pp.15.01246.

1123 Stein, Barry D., Karen L. Klomparens, and Raymond Hammerschmidt. 1992.
1124 "Comparison of Bromine and Permanganate as Ultrastructural Stains
1125 for Lignin in Plants Infected by the FungusColletotrichum

1126 Lagenarium." *Microscopy Research and Technique* 23 (3): 201–6.
1127 https://doi.org/10.1002/jemt.1070230302.

1128 Takano, Junpei, Mayuki Tanaka, Atsushi Toyoda, Kyoko Miwa, Koji Kasai,
1129 Kentaro Fuji, Hitoshi Onouchi, Satoshi Naito, and Toru Fujiwara. 2010.
1130 "Polar Localization and Degradation of Arabidopsis Boron
1131 Transporters through Distinct Trafficking Pathways." *Proceedings of*
1132 *the National Academy of Sciences of the United States of America*.
1133 https://doi.org/10.1073/pnas.0910744107.

1134 Ursache, R, T G Andersen, P Marhavy, and N Geldner. 2018. "A Protocol for
1135 Combining Fluorescent Proteins with Histological Stains for Diverse
1136 Cell Wall Components." *Plant J* 93 (2): 399–412.
1137 https://doi.org/10.1111/tpj.13784.

1138 Yamashita, Daichi, Satoshi Kimura, Masahisa Wada, and Keiji Takabe. 2016.
1139 "Improved Mäule Color Reaction Provides More Detailed Information
1140 on Syringyl Lignin Distribution in Hardwood." *Journal of Wood Science*
1141 62 (2): 131–37. https://doi.org/10.1007/s10086-016-1536-9.

1142 Zuo, Jianru, Qi-Wen W. Niu, and Nam-Hai H. Chua. 2000. "An Estrogen
1143 Receptor-Based Transactivator XVE Mediates Highly Inducible Gene
1144 Expression in Transgenic Plants." *The Plant Journal* 24 (2): 265–73.
1145 https://doi.org/10.1046/j.1365-313x.2000.00868.x.

1146

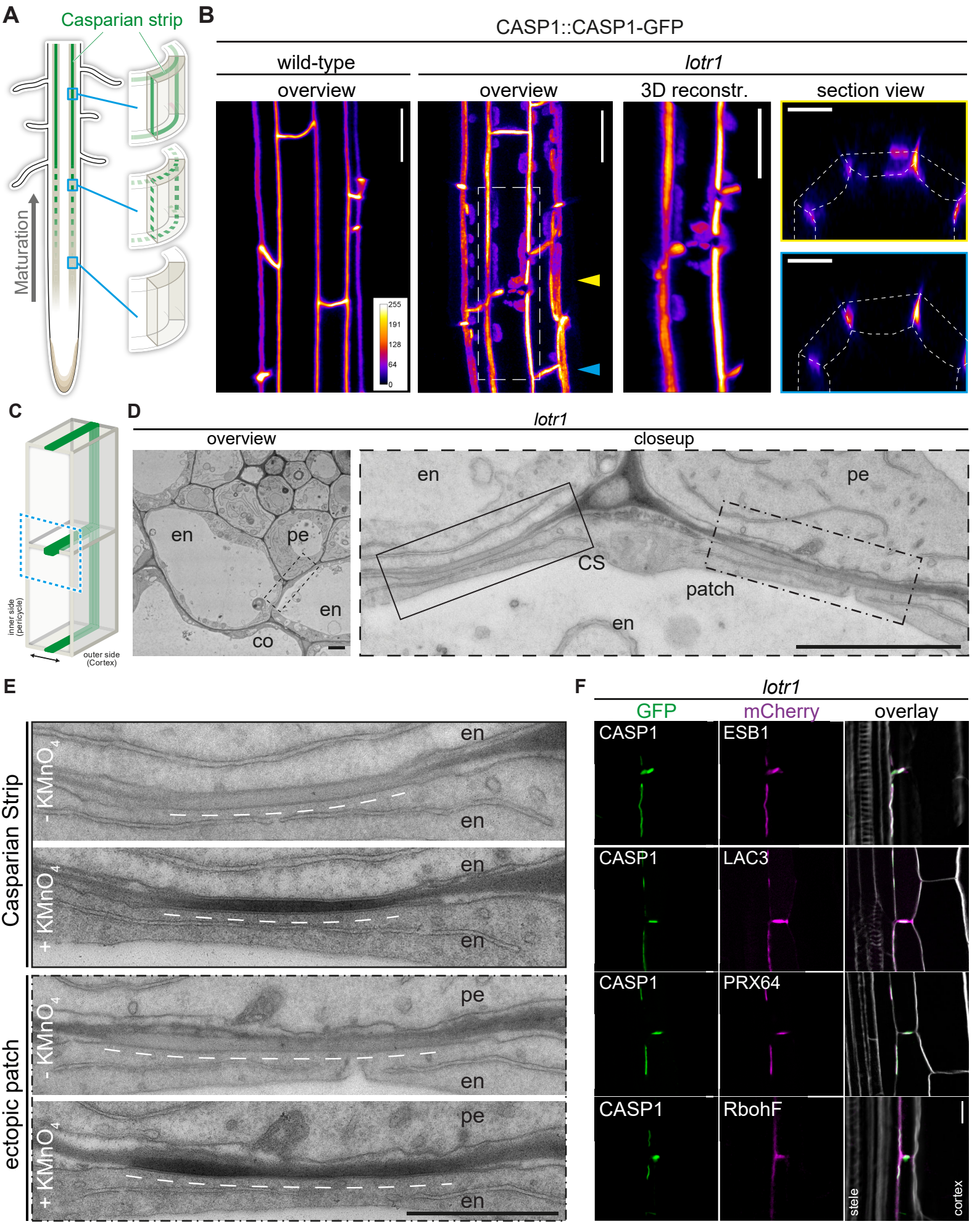
A
Casparian strip
Maturation
B
CASP1::CASP1-GFP
wild-type
lotr1
overview
overview
3D reconstr.
section view
255
191
128
64
0
C
inner side (pericycle)
outer side (Cortex)
D
lotr1
overview
closeup
en
pe
en
co
en
pe
CS
patch
en
E
lotr1
Casparian Strip
ectopic patch
- KMnO4
+ KMnO4
- KMnO4
+ KMnO4
en
en
en
en
pe
en
pe
en
F
lotr1
GFP
mCherry
overlay
CASP1
ESB1
CASP1
LAC3
CASP1
PRX64
CASP1
RbohF
stele
cortex

Fig. 1

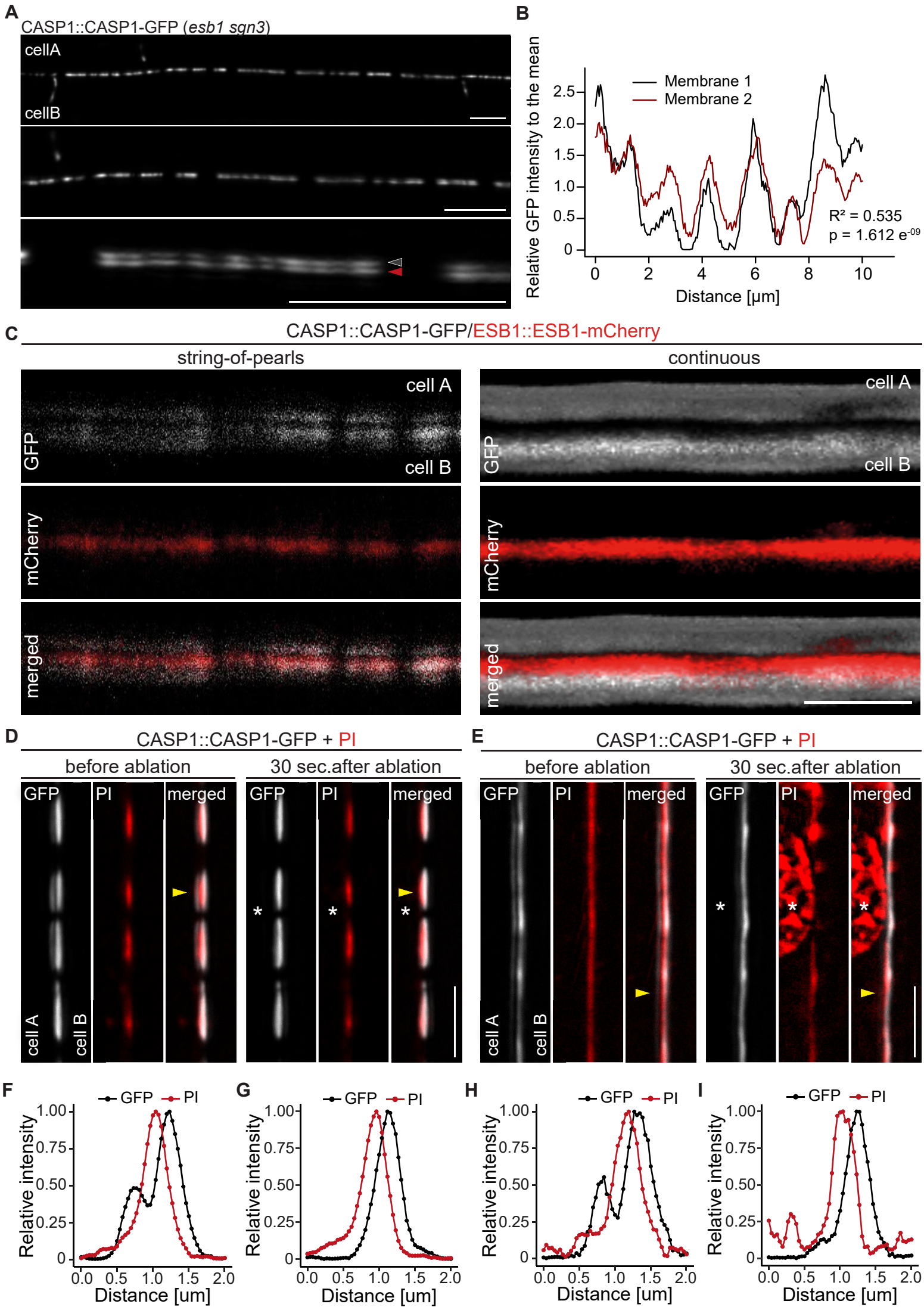
A
CASP1::CASP1-GFP (esb1 sqn3)
cellA
cellB
B
Membrane 1
Membrane 2
Relative GFP intensity to the mean
R² = 0.535
p = 1.612 e-09
Distance [µm]
C
CASP1::CASP1-GFP/ESB1::ESB1-mCherry
string-of-pearls
continuous
cell A
cell B
GFP
mCherry
merged
D
CASP1::CASP1-GFP + PI
before ablation
30 sec.after ablation
GFP
PI
merged
cell A
cell B
E
CASP1::CASP1-GFP + PI
before ablation
30 sec.after ablation
F
G
H
I
Relative intensity
Distance [um]

Fig. 2

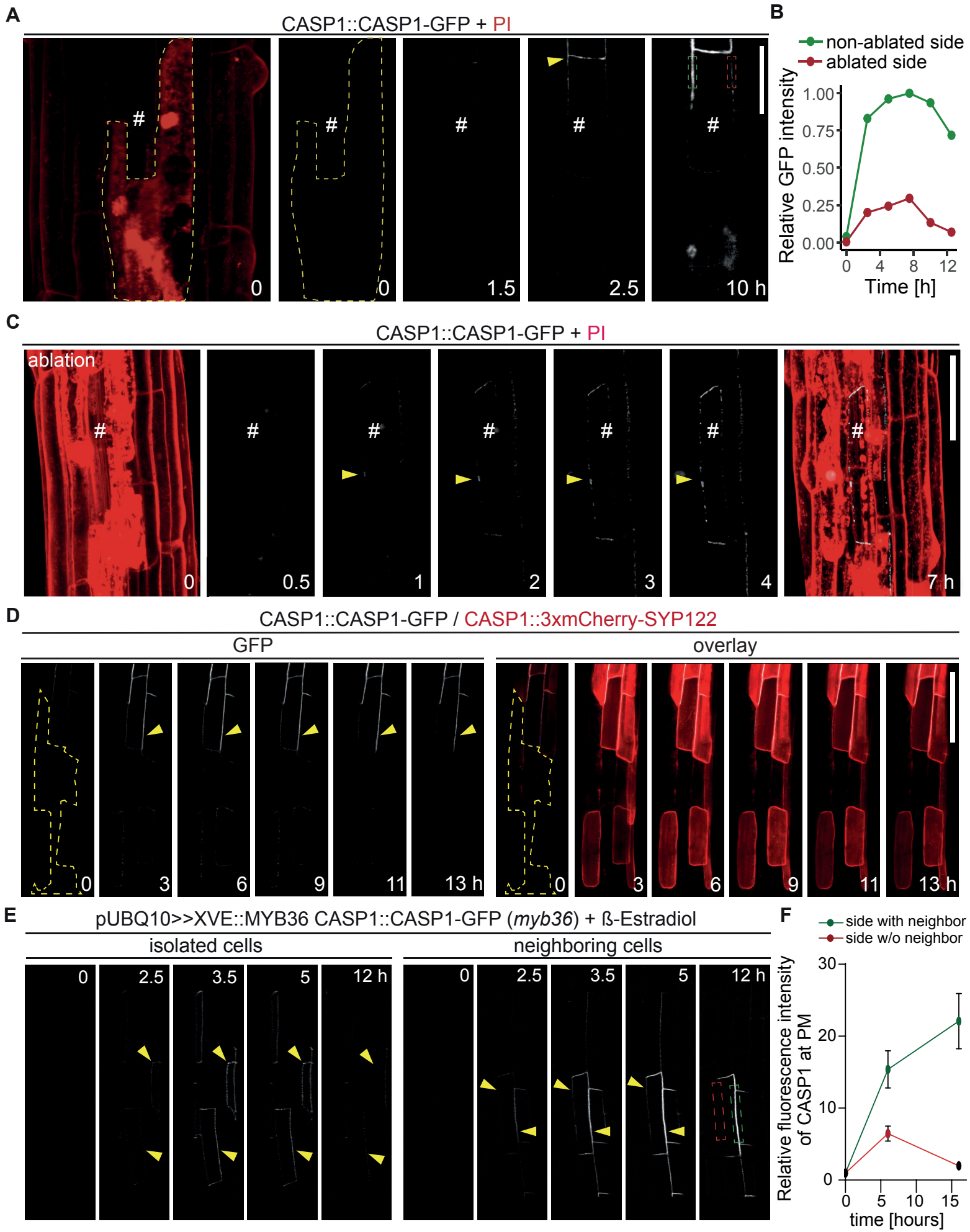
A
CASP1::CASP1-GFP + PI
#
0
0
1.5
2.5
10 h
B
non-ablated side
ablated side
Relative GFP intensity
1.00
0.75
0.50
0.25
0.00
0
4
8
12
Time [h]
C
CASP1::CASP1-GFP + PI
ablation
0
0.5
1
2
3
4
7 h
D
CASP1::CASP1-GFP / CASP1::3xmCherry-SYP122
GFP
overlay
0
3
6
9
11
13 h
E
pUBQ10>>XVE::MYB36 CASP1::CASP1-GFP (myb36) + ß-Estradiol
isolated cells
neighboring cells
0
2.5
3.5
5
12 h
F
side with neighbor
side w/o neighbor
Relative fluorescence intensity of CASP1 at PM
30
20
10
0
0
5
10
15
time [hours]

Fig. 3

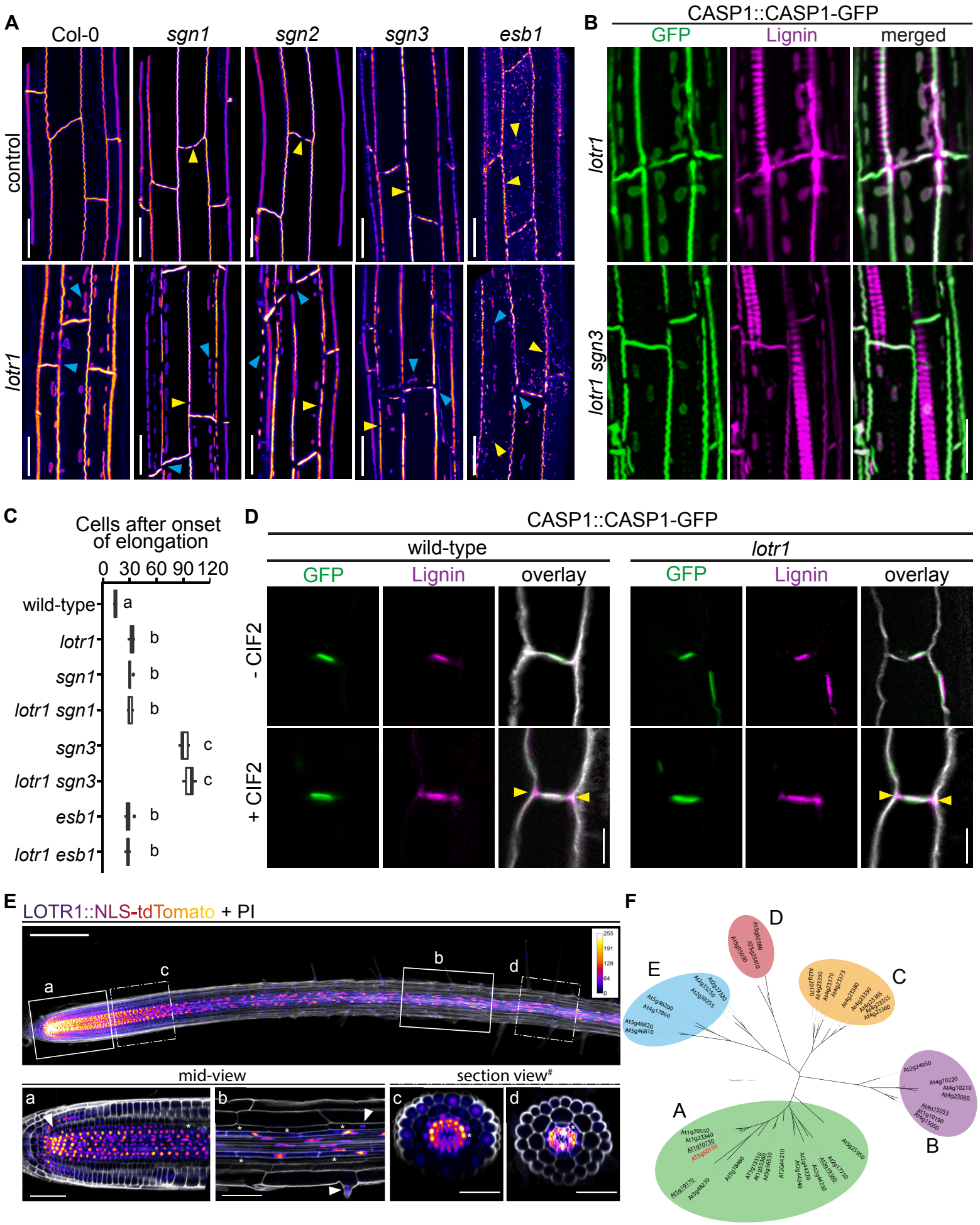
A
Col-0
sgn1
sgn2
sgn3
esb1
control
lotr1
B
CASP1::CASP1-GFP
GFP
Lignin
merged
lotr1
lotr1 sgn3
C
Cells after onset of elongation
0 30 60 90 120
wild-type
lotr1
sgn1
lotr1 sgn1
sgn3
lotr1 sgn3
esb1
lotr1 esb1
a
b
b
b
c
c
b
b
D
CASP1::CASP1-GFP
wild-type
lotr1
GFP
Lignin
overlay
- CIF2
+ CIF2
E
LOTR1::NLS-tdTomato + PI
a
c
b
d
mid-view
section view#
F
A
B
C
D
E

Fig. 4

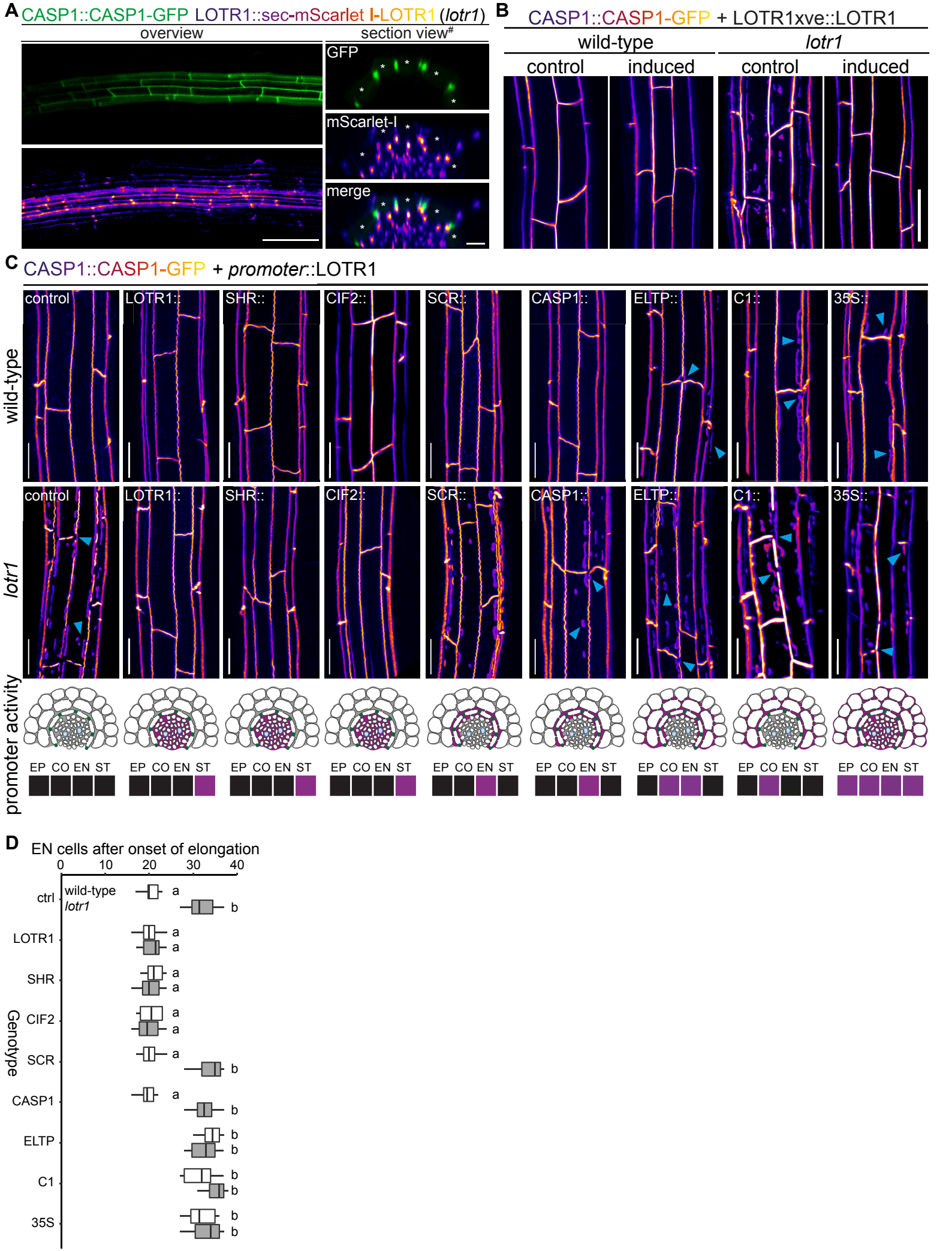
A
CASP1::CASP1-GFP LOTR1::sec-mScarlet I-LOTR1 (lotr1)
overview
section view#
GFP
mScarlet-I
merge
B
CASP1::CASP1-GFP + LOTR1xve::LOTR1
wild-type
lotr1
control
induced
control
induced
C
CASP1::CASP1-GFP + promoter::LOTR1
wild-type
lotr1
control
LOTR1::
SHR::
CIF2::
SCR::
CASP1::
ELTP::
C1::
35S::
promoter activity
EP CO EN ST
D
EN cells after onset of elongation
0
10
20
30
40
Genotype
ctrl
wild-type
lotr1
LOTR1
SHR
CIF2
SCR
CASP1
ELTP
C1
35S
a
b

Fig. 5

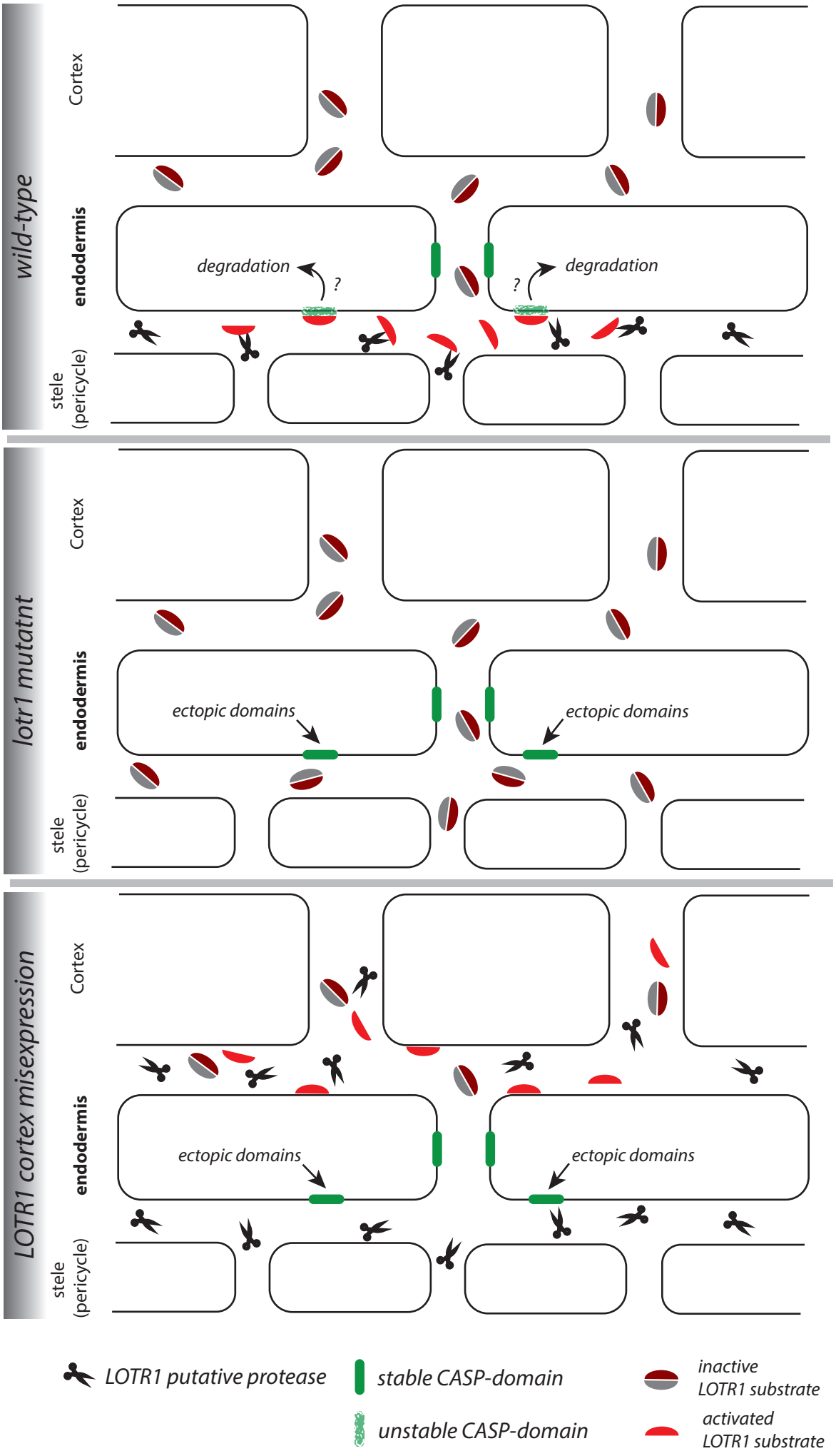
wild-type
Cortex
endodermis
stele
(pericycle)
degradation
?
?
degradation
lotr1 mutatnt
Cortex
endodermis
stele
(pericycle)
ectopic domains
ectopic domains
LOTR1 cortex misexpression
Cortex
endodermis
stele
(pericycle)
ectopic domains
ectopic domains
LOTR1 putative protease
stable CASP-domain
unstable CASP-domain
inactive
LOTR1 substrate
activated
LOTR1 substrate

Fig. 6